

Elena Martina Unterleutner, BSc

Growing graphene epitaxially on Ge(110) with plasma enhanced chemical vapor deposition

Marshall Plan Scientific Report

submitted to

Austrian Marshall Plan Foundation

Supervisor

Assoc.Prof. Dr. Anna Maria Coclite
Institute of Solid State Physics
Graz University of Technology

Co-supervisor

Assistant Professor Zakaria Al Balushi
Department of Materials Science and Engineering
University of California, Berkeley

Graz, June 2023

Abstract

Graphene is a two dimensional material with many promising technological applications, due to its exciting electronic properties. Ge(110) can be used to grow wafer-scale high-quality graphene epitaxially with chemical vapor deposition (CVD) with necessary process temperatures of up to 930 °C. Plasma enhanced CVD (PECVD) provides more freedom in the process conditions due to its increased reactivity. Shifting the required thermal energy to a second furnace in a thermal CVD process also enables lower deposition temperatures for a substrate.

This work aims at illustrating the influence of different process conditions on the deposited graphene films and their optimization with an emphasis on lower process temperatures with respect to commercial CVD processes. Graphene deposition was attempted by CVD, PECVD and CVD with two furnaces, using CH₄ and H₂ as precursors and Ge(110) as growth substrate. Raman spectroscopy, optical microscopy and scanning electron microscopy measurements were performed to characterize the deposited thin films.

Acknowledgements

First of all, I want to thank my supervisor Assoc. Prof. Anna Maria Coclite for making this thesis possible. I was extremely lucky to have her as my supervisor as she guided me through the work, motivated me and was always there for advice when necessary.

This master thesis was done in collaboration with Assistant Prof. Zakaria Y. Al Balushi from the University of California, Berkeley. I want to thank him especially for enabling this incredible opportunity and hosting me in his laboratory and involving me in such an interesting and exciting project. I also want to thank the rest of the research group, including Jiayun Liang, Healin Im, Bum Jun Kim, Ayush Gupta and Jennifer Toy for their valuable input and support.

I also want to thank all the other people in Berkeley, who made this time so special, with a special emphasis on the people living in the McGee Ave, the people from the bouldering group and everybody participating in the regular Taco Tuesdays.

I also want to express my deepest gratitude to the Marshall Plan Foundation, for their financial support enabling my research stay in Berkeley.

Furthermore, I am grateful of the support from my friends in Austria, especially Patricia and Flo. I also want to thank my boyfriend Paul, my sister Lisa and my parents for always being there for me and their support.

Contents

1	Fundamentals	1
1.1	Chemical Vapor Deposition	1
1.2	Plasma Enhanced Chemical Vapor Deposition	2
1.3	Epitaxy	4
2	Materials	5
2.1	Germanium	5
2.1.1	Surface Cleaning	6
2.2	Graphene	8
2.2.1	CVD of Graphene	9
2.2.2	PECVD of Graphene	15
3	Characterization	18
3.1	Raman Spectroscopy	18
3.1.1	Data Analysis	19
4	Setup and Experimental Methods	21
4.1	CVD	21
4.1.1	Experimental Setup	21
4.1.2	Experimental Workflow	23
4.2	PECVD	25
4.2.1	Experimental Setup	25
4.2.2	Experimental Workflow	26
4.3	Dual Furnace CVD	27
4.3.1	Experimental setup	27
4.3.2	Experimental Workflow	28
5	Results	31
5.1	Sample Cleaning	31
5.2	Single Furnace CVD	32
5.3	PECVD	41
5.4	Dual Furnace CVD	45
5.4.1	First Experimental Series	45
5.4.2	Second Experimental Series	51
5.4.3	Third Experimental Series	56
6	Conclusions and Outlook	68
	Bibliography	70

List of Figures

1.1.1	Sequential Steps of CVD. Reprinted from (1).	2
1.3.1	Possible forms of heteroepitaxial structures: Lattice matched, strained and relaxed. Reprinted from (1).	4
2.1.1	Diamond crystal structure of face-centered cubic space lattice with two atom basis. Reprinted from (4).	5
3.1.1	Raman spectra of pristine graphene (top) and defective graphene (bottom). Reprinted from (38).	19
3.1.2	Raman spectra of graphene (top) and graphite (bottom). Reprinted from (2).	19
4.1.1	Schematic layout of the CVD reactor.	22
4.2.1	Schematic layout of the PECVD reactor. The dashed line indicates a RF power transmission cable.	26
4.3.1	Schematic layout of the dual furnace CVD reactor.	28
5.1.1	Optical microscope images of polished Ge(110) surface after degreasing cleaning step, 100x magnification and scale bar of 4 μm	31
5.1.2	Optical microscope images of the polished Ge(110) surface after H ₂ annealing cleaning step, 100x magnification and scale bar of 4 μm	32
5.2.1	Optical microscope images of graphene on Ge(110) samples at 600 °C single furnace CVD deposition temperature, 100x magnification and 4 μm scale bar.	33
5.2.2	Optical microscope images of graphene on Ge(110) samples at 700 °C single furnace CVD deposition temperature, 100x magnification and 4 μm scale bar.	33
5.2.3	Optical microscope images of graphene on Ge(110) samples at 800 °C single furnace CVD deposition temperature, 100x magnification and 4 μm scale bar.	34
5.2.4	Averaged Raman spectra of graphene on Ge(110) samples at 600 °C single furnace CVD deposition temperature.	35
5.2.5	Averaged Raman spectra of graphene on Ge(110) samples at 700 °C single furnace CVD deposition temperature.	36
5.2.6	Averaged Raman spectra of graphene on Ge(110) samples at 800 °C single furnace CVD deposition temperature.	38
5.2.7	Raman spectra of graphene on Ge(110) samples at 800 °C single furnace CVD deposition temperature and 100 sccm CH ₄ and 100 sccm H ₂ , focused on the etch pits.	39

List of Figures

5.3.1	Optical microscope images of graphene on Ge(110) samples at 800 °C PECVD deposition temperature, 100x magnification, and 4 μm scale bar.	42
5.3.2	Optical microscope images of graphene on Ge(110) sample at 900 °C PECVD deposition temperature and 20 sccm CH ₄ , 20 sccm H ₂ and 10 sccm Ar, 100x magnification and scale bar of 4 μm.	42
5.3.3	Averaged Raman spectra of graphene on Ge(110) samples at 800 °C PECVD deposition temperature.	43
5.3.4	Averaged Raman spectra of graphene on Ge(110) samples with 900 °C PECVD deposition temperature and 20 sccm CH ₄ , 20 sccm H ₂ and 10 sccm Ar.	44
5.4.1	Optical microscope images of graphene on Ge(110) samples grown by dual furnace CVD, 1 st furnace temperature 1000 °C, 2 nd furnace temperature 800 °C, 100x magnification and 4 μm scale bar.	45
5.4.2	Optical microscope images of graphene on Ge(110) samples grown at 10 Torr pressure by dual furnace CVD, 1 st furnace temperature 1000 °C, 2 nd furnace temperature 800 °C, 100x magnification and 4 μm scale bar.	46
5.4.3	Averaged Raman spectra of graphene on Ge(110) samples grown by double furnace CVD, 1 st furnace temperature 1000 °C, 2 nd furnace temperature 800 °C.	48
5.4.4	Optical microscope images of graphene on Ge(110) samples grown by dual furnace CVD, 100x magnification and 4 μm scale bar.	51
5.4.5	SEM images of graphene on Ge(110) samples grown by dual furnace CVD.	52
5.4.6	Averaged Raman spectra of graphene on Ge(110) samples grown by dual furnace CVD.	54
5.4.7	SEM images of graphene on Ge(110) samples grown by dual furnace CVD, H ₂ /CH ₄ ratio series, 1 μm scale bar.	57
5.4.8	SEM images of graphene on Ge(110) samples grown by dual furnace CVD, time series.	58
5.4.9	SEM images of graphene on Ge(110) samples grown by dual furnace CVD, pressure series.	59
5.4.10	SEM images of graphene on Ge(110) samples grown by dual furnace CVD, temperature series, 1 μm scale bar.	60
5.4.11	Averaged Raman spectra of graphene on Ge(110) samples grown by dual furnace CVD, H ₂ /CH ₄ ratio series.	62
5.4.12	I _D /I _G ratios, I _{2D} /I _G ratios and FWHMs of the 2D peaks of the H ₂ /CH ₄ ratio series. Error bars are σ.	62
5.4.13	Averaged Raman spectra of graphene on Ge(110) samples grown by dual furnace CVD, time series.	63
5.4.14	I _D /I _G ratios, I _{2D} /I _G ratios and FWHMs of the 2D peaks of the time series. Error bars are σ.	63
5.4.15	Averaged Raman spectra of graphene on Ge(110) samples grown by dual furnace CVD, pressure series.	64

List of Figures

5.4.16	Averaged Raman spectra of graphene on Ge(110) samples grown by dual furnace CVD, temperature series.	64
5.4.17	I_D/I_G ratios, I_{2D}/I_G ratios and FWHMs of the 2D peaks of the temperature series. Error bars are σ	65

List of Tables

4.1	Devices and instruments used for the experimental setup.	22
4.2	Parameters during the CVD graphene deposition step.	25
4.3	Parameters during the graphene deposition step of the first series of experiments with dual furnace CVD.	29
4.4	Parameters during the graphene deposition step of the second series of experiments using dual furnace CVD.	30
4.5	Parameters during the graphene deposition step of the third series of experiments using dual furnace CVD.	30
5.1	Background subtraction parameters asymmetric factor, threshold, smoothing factor, and number of iterations for the asymmetric least squares method and relative standard deviation for the Raman spectra of graphene on Ge(110) samples with 600 °C single furnace CVD deposition temperature.	36
5.2	Background subtraction parameters asymmetric factor, threshold, smoothing factor, and number of iterations for the asymmetric least squares method and relative standard deviation for the Raman spectra of graphene on Ge(110) samples with 700 °C single furnace CVD deposition temperature, intact surface.	37
5.3	Background subtraction parameters asymmetric factor, threshold, smoothing factor, and number of iterations for the asymmetric least squares method and relative standard deviation for the Raman spectra of graphene on Ge(110) samples with 700 °C single furnace CVD deposition temperature, etch pits.	37
5.4	Background subtraction parameters asymmetric factor, threshold, smoothing factor, and number of iterations for the asymmetric least squares method and relative standard deviation for the averaged Raman spectra of graphene on Ge(110) samples with 800 °C single furnace CVD deposition temperature, intact surface.	40
5.5	Background subtraction parameters asymmetric factor, threshold, smoothing factor, and number of iterations for the asymmetric least squares method and relative standard deviation for the Raman spectra of graphene on Ge(110) samples with 800 °C single furnace CVD deposition temperature, etch pits	40
5.6	Lorentz function fit parameters y-offset, peak center, area, FWHM and derived peak height with their standard errors for the fitted peaks in Figure 5.2.7c.	40

5.7	Background subtraction parameters asymmetric factor, threshold, smoothing factor and number of iterations for the asymmetric least square method and relative standard deviation for the averaged Raman spectra of graphene on Ge(110) samples with 800 °C and 900 °C PECVD deposition temperature, intact surface.	44
5.8	Background subtraction parameters asymmetric factor, threshold, smoothing factor and number of iterations for asymmetric least square method and relative standard deviation for the averaged Raman spectra of graphene on Ge(110) samples with 800 °C and 900 °C PECVD deposition temperature, etch pits.	44
5.9	Relative standard deviation for the averaged Raman spectra of graphene on Ge(110) samples grown with dual furnace CVD, 1 st furnace temperature 1000 °C, 2 nd furnace temperature 800 °C.	49
5.10	Lorentz function fit parameters y-offset, peak center, area, FWHM and derived peak height and their standard errors for CH ₄ :H ₂ = 10:10 sccm at 1 Torr grown by dual furnace CVD, 1 st furnace temperature 1000 °C, 2 nd furnace temperature 800 °C.	49
5.11	Lorentz function fit parameters y-offset, peak center, area, FWHM and derived peak height and their standard errors for CH ₄ :H ₂ = 10:10 sccm at 10 Torr grown by dual furnace CVD, 1 st furnace temperature 1000 °C, 2 nd furnace temperature 800 °C.	49
5.12	Lorentz function fit parameters y-offset, peak center, area, FWHM and derived peak height and their standard errors for CH ₄ :H ₂ = 10:25 sccm at 10 Torr grown dual furnace CVD, 1 st furnace temperature 1000 °C, 2 nd furnace temperature 800 °C	50
5.13	Lorentz function fit parameters y-offset, peak center, area, FWHM, and derived peak height and their standard errors for the sample cleaned by the degreasing method only, grown by single furnace CVD at 800 °C, near the etch pits.	55
5.14	Lorentz function fit parameters y-offset, peak center, area, FWHM, and derived peak height and their standard errors for the sample cleaned by the degreasing method only, grown by single furnace CVD at 800 °C, etch pits.	55
5.15	Lorentz function fit parameters y-offset, peak center, area, FWHM, and derived peak height and their standard errors for the sample grown by single furnace CVD at 800 °C.	55
5.16	Lorentz function fit parameters y-offset, peak center, area, FWHM, and derived peak height and their standard errors for the sample grown by dual furnace CVD , 1 st furnace temperature 800 °C, 2 nd furnace temperature 800 °C.	55
5.17	Lorentz function fit parameters y-offset, peak center, area, FWHM, and derived peak height and their standard errors for the samples grown by dual furnace CVD, H ₂ /CH ₄ ratio series.	65

5.18	Background subtraction parameters asymmetric factor, threshold, smoothing factor and number of iterations for asymmetric least square method and relative standard deviation for the averaged Raman spectra of graphene on Ge(110) samples grown by dual furnace CVD, H ₂ /CH ₄ ratio series.	66
5.19	Lorentz function fit parameters y-offset, peak center, area, FWHM, and derived peak height and their standard errors for the samples grown by dual furnace CVD, time series.	66
5.20	Background subtraction parameters asymmetric factor, threshold, smoothing factor and number of iterations for asymmetric least square method and relative standard deviation for the averaged Raman spectra of graphene on Ge(110) samples grown by dual furnace CVD, time series.	66
5.21	Background subtraction parameters asymmetric factor, threshold, smoothing factor and number of iterations for asymmetric least square method and relative standard deviation for the averaged Raman spectra of graphene on Ge(110) samples grown by dual furnace CVD, pressure series.	67
5.22	Lorentz function fit parameters y-offset, peak center, area, FWHM, and derived peak height and their standard errors for the samples grown by dual furnace CVD, temperature series.	67
5.23	Background subtraction parameters asymmetric factor, threshold, smoothing factor and number of iterations for asymmetric least square method and relative standard deviation for the averaged Raman spectra of graphene on Ge(110) samples grown by dual furnace CVD, temperature series.	67

1 Fundamentals

The following chapter describes the basics of chemical vapor deposition, plasma-enhanced chemical vapor deposition, and epitaxy to provide a basic understanding of the processes involved in this thesis. A more detailed description can be found in chapters 4, 6, and 8 of the second edition of *Materials Science of Thin Films: Deposition & Structure* by Milton Ohring (1). A review letter by Saeed et. al. also provides great insight into the topic, focusing on the synthesis of graphene using CVD processes. (2)

1.1 Chemical Vapor Deposition

Chemical vapor deposition (CVD) is the process of depositing a non-volatile solid on a substrate at the atomic level by chemical reactions of volatile compounds of a material with other gases. Unlike physical vapor deposition (PVD), the gas species react with each other to form new species, rather than relying solely on material transport from a condensed phase evaporant. Because CVD processes do not require a vacuum or very high electrical power, they were commercially available before PVD. CVD processes were used a century ago to produce tungsten-coated carbon filaments to extend the life of filaments used in incandescent lamps. Today, CVD processes have a wide range of applications, such as in the semiconductor industry, but also in the manufacture of nuclear reactor parts, ball bearings and rocket engines. The advantages of CVD include the variety of materials that can be deposited as films or coatings with desired properties in crystalline or amorphous form, the affordable cost factor of the equipment and its operation, and its compatibility with other processing steps. Several variants of CVD have been developed, such as low pressure (LPCVD), atmospheric pressure (APCVD), laser enhanced (LECVD), or plasma enhanced chemical vapor deposition (PECVD).

The basic process steps are the same for each CVD method and are shown in Figure 1.1.1. First, the reactants are transported convectively and diffusely from the gas inlets to the reaction zone. Reactive species and by-products are formed in the gas phase by chemical reactions. The initial reactants and their products are transported to the substrate surface where they are chemically and physically adsorbed and diffused. The surface catalyzes heterogeneous reactions leading to the formation of the film. The volatile by-products of the reactions on the surface desorb and are transported away from the reaction zone by convection and diffusion.

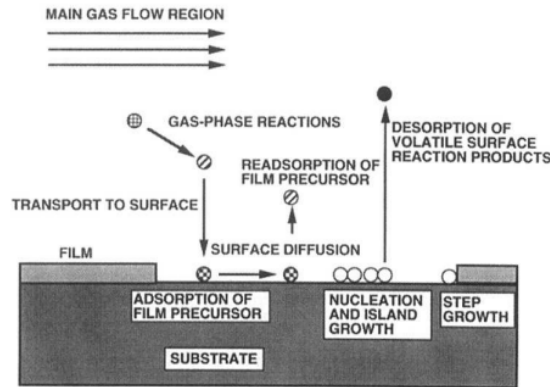


Figure 1.1.1: Sequential Steps of CVD. Reprinted from (1).

The two main categories of CVD processes are thermal CVD processes and plasma-enhanced CVD processes. In thermal CVD, the thermal energy activates the reactions in the gas and on the surface. In PECVD processes, the plasma activates the reactions. However, the resulting deposited films can differ in terms of film properties, structure, and composition, even with similar input gases.

Thermal CVD can again be divided into categories such as high and low temperature, hot and cold wall, low and atmospheric pressure, and closed and open. However, all of these systems have equipment to introduce and meter the involved gases into the reactor, provide heat to the substrate, and remove the remaining volatile species.

LPCVD is typically performed in the 1-10 mTorr pressure range and has advantages over APCVD such as higher deposition rates, fewer contamination problems, fewer pinhole defects, better film thickness uniformity, lower particle density, better stoichiometry control, and better step coverage. When the CVD process is operated at pressures between 1-100 Torr, the term reduced pressure CVD (RPCVD) is used. (1)

1.2 Plasma Enhanced Chemical Vapor Deposition

In PECVD reactors, chemical gas reactions and film deposition occur simultaneously with a sustained glow discharge plasma. The driving force behind the development of PECVD processes was the semiconductor industry, as PECVD enabled the low-temperature deposition of silicon nitride passivation layers on microelectronic devices. Commercial thermal CVD processes require temperatures well above 300 °C, which is too hot for finished IC chips.

Most glow discharge plasmas in PECVD systems are excited by a radio frequency (RF) field, with RF frequencies typically ranging from 100 kHz to 40 MHz. The gas environment is typically maintained at a reduced pressure between 50 mTorr and 5 Torr. Gas molecules are broken down into a variety of species such as atoms, ions, free radicals, molecular fragments, or molecules in excited or ground states due to the energetic discharge of the plasma. The interaction of all these reactive components allows chemical reactions to occur at lower temperatures than in thermal activation processes.

The main distinguishing category for PECVD processes is the excitation source, which can be RF or microwave, and the type of coupling, which can be inductive or capacitive. Depending on these characteristics, several reactor configurations are possible. The simplest reactor configuration, which was used in this thesis, is a tube reactor with a coil wrapped around the tube. The coupling is inductive, for capacitive coupling external electrode plates must be used. The gases flowing through the tube are ionized and reactions occur, resulting in the deposition of solid films on substrates placed in the tube. For both inductively and capacitively coupled PECVD processes, a symmetrical potential is developed on the chamber wall in this setup. This potential can sputter wall atoms that can be incorporated into the growing film. Thus, high potentials are avoided. When the product and reactant gases, the plasma and the substrate are all kept together in the same chamber, the process is referred to as conventional or direct PECVD. The disadvantage of this method is the higher possibility of unwanted etching and deposition, which is limited when substrates and plasma zone are physically separated.

Predicting the kinetics of film deposition or etching processes is often only possible with computer simulations due to the complexity of plasma processes. One approach is to divide the process into three parts:

1. Electron kinetics: The electric and magnetic fields are calculated or assumed to obtain information about the electron impact cross sections and rate constants. The sheath properties and the spatially and temporally varying electron density are modeled and calculated to obtain information about the various electron-particle collision cross sections.
2. Plasma chemistry: The concentration of charged species, neutrals, and radicals as a function of time and space is modeled while satisfying the physical rules of energy, charge, and mass conservation. All reactant and product species are treated separately. Information on their motion by drift, convective gas transport, and diffusion is also linked to chemical reactions induced by collisions using rate constants derived from the electron kinetics model.
3. Surface Reactions: The interactions of the surface layers of the substrate with the bombarding radicals and ions are modeled, as well as the net sticking rates of different gas components and the kinetics of adsorption. This step attempts to understand the chemical and physical mechanisms in etching and film deposition processes.

All three parts are interrelated and benefit from additional experimental data such as spectral information, discharge breakdown fields or light output from added actinometer gases. (1)

1.3 Epitaxy

Epitaxy is the extended single crystal film formation of a crystalline substrate beyond its surface. It plays a major role in semiconductor thin film device technology, but less so in other areas such as hard, protective and optical thin film coatings, and thin films used for information storage, display and recording. For industrial applications today, the growth of defect-free epitaxial films is of great importance.

The two main types of epitaxy are homoepitaxy and heteroepitaxy. In homoepitaxy, the substrate and the deposited film are the same material, while in heteroepitaxy different materials are used. The latter has more applications in our world. When different materials are used, their lattice parameters are usually different, unlike in homoepitaxy where the lattice parameters are necessarily matched and no strain is introduced due to lattice mismatch. For small mismatches, the interface structure becomes similar to that of homoepitaxy, but differences in thermal expansion and chemistry also play an important role in the electronic properties and the resulting interface. Figure 1.3.1 illustrates the schematic differences of lattice structures in epitaxy. Homoepitaxy is structurally similar to lattice-matched heteroepitaxy.

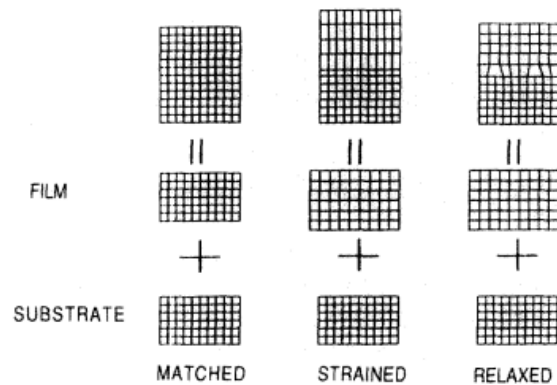


Figure 1.3.1: Possible forms of heteroepitaxial structures: Lattice matched, strained and relaxed. Reprinted from (1).

Strained and relaxed heteroepitaxial structures develop from larger lattice parameter differences. However, strained lattices generally predominate in the early stages of film formation until the strain can no longer accommodate the differences and dislocation defects develop. This is often observed for materials with the same crystal structure and is referred to as pseudomorphic film growth. Common defects in epitaxial films are screw dislocations, misfit dislocations, stacking defects, oval defects, dislocation loops from dopants, precipitates or impurities, and low angle grain boundaries and twins. (1)

2 Materials

This chapter introduces the basics of graphene and germanium and their role in the deposition of the thin films, as well as how graphene has been deposited on germanium via CVD and PECVD in the literature so far.

2.1 Germanium

Germanium is a semiconductor and has a diamond structure, which is a face-centered cubic (fcc) lattice. In the primitive basis of this structure, there are two identical atoms at coordinates 000 and $\frac{1}{4}\frac{1}{4}\frac{1}{4}$ associated with each fcc lattice point. The conventional unit cube therefore contains 8 atoms, as shown in figure 2.1.1. The atoms with 4 nearest and 12 next nearest neighbors also have a tetrahedral bonding characteristic. The length of the conventional cubic cell a is 5.658 Å. (3)

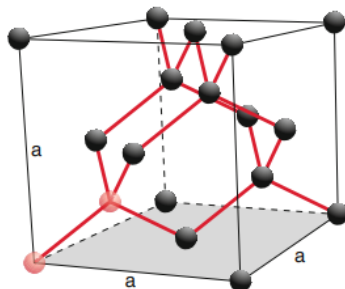


Figure 2.1.1: Diamond crystal structure of face-centered cubic space lattice with two atom basis. Reprinted from (4).

The unstructured Ge(110) surface has rectangular symmetry and ziczac alignment of the atoms in the $[\bar{1}10]$ direction. Before relaxation, all atomic layers are evenly spaced and the surface atoms have tetrahedral bonds in the (110) plane with their two nearest neighbors in the plane above and below. The surface reconstruction of the Ge(110) surface depends on the annealing temperature and can be either a (16×2) structure or a $c(8 \times 10)$ structure at temperatures below 380 °C and above 430 °C. On both reconstructed surfaces, pentagonal clusters of adatoms form rows and $\{17\ 15\ 1\}$ facets at step edges, which run in the same direction as the rows on the (16×2) structure. In the (16×2) reconstruction, the top layer of (110) atoms, which would alternate across double rows of adatoms in the reconstruction, is missing. Instead, the adatom cluster double rows go up and then down in the layer below the surface of Ge(110). The $c(8 \times 10)$ reconstruction differs in that the double lines are all in the same (110) plane.

At temperatures of 800 °C, the $c(8 \times 10)$ reconstruction was not observed, and rapid quenching to room temperature resulted in a surface with a new (8×2) phase, $c(8 \times 10)$ terraces, and $\{17\ 15\ 1\}$ facets. (5)

2.1.1 Surface Cleaning

The first step in successfully growing high quality graphene on Ge(110) will be to ensure clean germanium substrates, as carbon impurities and also other impurities such as oxygen can prevent the growth of high quality graphene. (8)

Relatively little information has been published on the cleaning of the Ge(110) surface, as most of the literature focuses on the Ge(001) surface. However, it is assumed that the same cleaning principles apply.

In the environment, germanium forms an oxide layer of GeO_2 and suboxides GeO_x , $x < 2$. GeO_2 is the most common and can exist in amorphous phases, water soluble hexagonal phases, or water insoluble rutile phases. GeO is generally water insoluble and thermally more stable than the former. However, all germanium oxides are thermally desorbed when the germanium surface is heated to temperatures of 390-600 °C under vacuum conditions.

Various cleaning methods for germanium include ultraviolet (UV) light, plasma exposure, ion sputtering, and wet etching. (9)

UV Light and Plasma Exposure

UV light and plasma exposure share the same chemical principle of breaking organic bonds such as C-C and C-H and producing highly reactive oxygen species that bond with the remaining organic radicals on the surface to form more volatile species such as H_2O , CO_2 and CO . Furthermore, a thin oxide passivation layer is formed due to the oxidation of the surface, which can be advantageous when used as an *ex situ* cleaning method. However, the main advantage of these cleaning methods is the absence of hazardous chemical waste. (9) Cleaning with UV light has shown results of nearly carbon and oxide free surfaces when the treatment follows an ultrasonic degreasing step and a deionized water rinse step or several cycles of wet etching. Subsequent thermal annealing under vacuum conditions is required to remove the oxide passivation layer. (10) (11) (12)

Oxygen plasma cleaning gives similar results, but can result in a rough surface. (13) (14) The use of hydrogen plasma or hydrogen annealing has the advantage of lower possible process temperatures due to the H_2 reacting with carbon and volatilizing oxides at the same time. A hydrogen passivation layer can also be obtained. However, even after previous cleaning steps including UV light and wet etching, some carbon and oxygen residues may remain. (9) (15) (16)

Hydrogen Annealing

Molecular hydrogen adsorbs dissociatively on germanium and hydrogen annealing of germanium can lead to catalytic hydrogenation of chemisorbed carbon contaminants and their desorption. Important parameters are temperature, annealing time and pressure. Low hydrogen pressures can lead to the formation of deep pyramidal etch pits and a system of polymerized carbons. With increasing pressure, these pits become shallower and rounder in shape. The etch pits are believed to form in the vicinity of threading dislocations where the topographic depressions induce preferential evaporation. On a clean surface, these pits would be filled by diffusing germanium adatoms. However, carbon impurities can block diffusion pathways and impede the refilling process. As the hydrogen dose is increased, the carbon impurities are reduced and the mobility of the adatoms is subsequently increased, resulting in the change of the observed etch pits. A decrease in temperature also results in slower carbon removal. Removal of carbon contamination is achieved by hydrogen annealing, and a successful process results in etch pit and particle free surfaces. In CVD processes, a hydrogen annealing step is often implemented in the heating step to the desired growth temperature. Better results can be achieved by separating these steps to allow for different process parameters such as temperature and pressure. (8)

Ion Sputtering

Ion sputtering in combination with wet etching and subsequent annealing can produce surfaces that are almost free of organic contamination. Several cycles of sputtering and annealing are therefore required. Thermal annealing is a critical step to heal the rough and amorphous surface. However, defects and protrusions may remain. The best results with this cleaning method are achieved with a subsequent germanium homoepitaxy step, resulting in atomically smooth and contamination-free Ge surfaces. Overall, this cleaning method is not practical considering the very long process times of multiple sputtering and annealing cycles and germanium regrowth. (9)

Wet Etching

Most cleaning methods include at least one cycle of wet etching. Most wet etching methods include a step of degreasing the germanium substrate, dissolving the native oxide layer and removing organic and metal contaminations on the surface, and forming a new passivation layer on the surface to prevent new contaminations from the environment, since it is an *ex situ* cleaning method. The ideal etchant should not increase the surface roughness by high germanium consumption, nor should it have high anisotropic properties, which can lead to undesired etching behavior. Ideally, the newly introduced passivation layer can be easily removed *in situ* by thermal desorption. An unavoidable disadvantage of chemical etching is the generation of chemical waste, which often has toxic and hazardous properties. (9) In general, most of the wet etching cleaning methods established in the semiconductor industry and widely used for silicon, such as CARO, SC1, SC2 or DDC, result in too extensive

etch rates in the case of germanium and are not suitable for cleaning germanium wafers. (17)

At least for Ge(001), rinsing with deionized (DI) water already falls into the category of wet etching, since it dissolves the GeO_2 that is always present on germanium surfaces exposed to air. However, it does not completely remove the suboxides on the germanium surface and may increase the surface roughness. It does not remove organic contaminants and does not passivate the surface, resulting in immediate regrowth of an oxide layer in the environment. (9)

Hydrofluoric acid (HF) is widely used in the semiconductor industry for cleaning purposes. In the case of Ge(001) it removes the GeO_2 , but leaves residual sub-oxides and organic impurities. The high etch rates also result in a higher surface roughness than in the as-received condition. The passivation layer consists of a hydrogen termination which increases with the HF concentration used. However, the hydrogen passivation layer is not stable in the environment, resulting in further carbon contamination and oxide regrowth on the time scale of minutes. (18) (19) (20) (21)

Hydrochloric acid (HCl) is able to completely remove oxides and carbon contaminants from the germanium surface and does not significantly increase the surface roughness. The passivation layer consists of a Cl-terminated surface, which undergoes re-oxidation on the same time scale as the H-terminated surface resulting from wet etching with HF.

Other acids, such as hydrobromic acid (HBr) and hydroiodic acid (HI), produce more stable passivation layers that can be removed by DI rinsing or thermal annealing under vacuum conditions. (19)

Ammonium hydroxide (NH_4OH) is able to completely remove germanium oxides and carbon from the surface like HCl, but the resulting surface roughness is slightly higher than HCl. However, it does not form a passivation layer by itself, so additional chemicals are needed. Hydrogen peroxide (H_2O_2) has been found to introduce a chemical oxide layer that can serve as a passivation layer and is removed by thermal annealing *in situ*, but other passivations such as S-passivation using $[(\text{NH}_4)_2\text{S}]$ are also possible. (22) (23) (24) (25)

2.2 Graphene

Graphene is a two-dimensional material consisting of a single layer of hexagonally arranged sp^2 hybridized carbon atoms and defines the elementary building block of graphite. The interatomic distance is 1.42 \AA in the tightly packed honeycomb lattice (2) and the height of monolayer graphene is 3.35 \AA (26). Research on graphene is a relatively young field, and one of the cornerstones was the exfoliation of graphene from bulk graphite in 2004. What keeps research on this material going for decades is the plethora of interesting properties like the theoretical specific surface area of $2630 \text{ m}^2/\text{g}$, a high Young's modulus of 1 TPa for defect-free single layer graphene, an ultrahigh electron mobility of $2 \times 10^5 \text{ cm}^2/\text{Vs}$ for suspended graphene, an exceptional thermal conductivity of 3500-5000 W/mK, and an exceptional electrical conductivity with critical current densities of 10^8 A/cm^2 . These special properties in strength, transmittance, conductivity and flexibility make it a promising candidate in many technological applications in different fields. Therefore, it is essential to find a way

to produce high quality graphene with as few defects and impurities as possible and with large grain sizes or even as uniform single crystals over wafer scales at commercial scale manufacturability. Various methods have been developed, such as mechanical and liquid phase exfoliation, silicon carbide sublimation, and chemical vapor deposition (CVD). Thermal/catalytic CVD uses graphene growth substrates and a hydrocarbon gas source. One way is to use carbon diffusion and segregation in a metal substrate with high carbon solubility. The other way, which is also the case with germanium where the solubility of carbon extremely small with $\langle 0.1\%$ in bulk germanium (7), is to use surface adsorption in substrates with low carbon solubility. This method has shown the best results so far. (2)

2.2.1 CVD of Graphene

Graphene synthesis using CVD methods depends on many different processing parameters such as temperature, pressure, precursor type, wall and substrate temperature, gas flow state, activation type, and deposition time.

A variety of precursors have been successfully used in the synthesis of graphene by CVD methods. Solid precursors such as poly methyl methacrylate (PMMA) can be spin-coated onto a substrate and loaded directly into the CVD reactor. Graphene film formation is then achieved by thermal sublimation. Liquid precursors such as hexane can be vaporized and introduced into the chamber with bubblers. The more common and easier to control type of precursor are gaseous carbon precursors such as methane (CH_4) gas, which was also used in this work. This precursor is introduced into the reactor via gas delivery systems.

Different energy sources used to activate film growth include hot wall, cold wall, and plasma enhanced CVD. One of the methods used in this thesis is hot wall CVD, where a furnace heats the chamber and growth substrate to a desired temperature for annealing and decomposition of the precursor. In most research a metal substrate such as copper (Cu) is used, in this thesis germanium (Ge) was chosen for the substrate. The substrate is placed in the quartz tube and annealed in a hydrogen atmosphere at reduced or atmospheric pressure to increase the grain size of the substrate and to reduce metal oxide films on the substrate. To grow graphene, hydrocarbon gas mixed with hydrogen in a certain ratio flows through the tube. Partial pressures are controlled by the reactor pressure or by introducing inert gases such as nitrogen (N) or argon (Ar) into the mixture. After the growth step, the furnace is turned off and the substrate is cooled to room temperature under a continuous flow of gas, often hydrogen, which can also be mixed with an inert gas. This helps to obtain a continuous monolayer of graphene by avoiding aggregation of carbon in the substrate surface, which could lead to bulk graphite or multilayer graphene.(2) Graphene synthesis with CVD can be divided into the following steps(2):

1. Convective transport of reactants in a gas stream
2. Thermal activation of reactants
3. Diffusive transport of reactants
4. Surface adsorption of reactants

5. Surface processes: Catalytic decomposition of CH_4 on the substrate surface and adsorption of carbon atoms at attachment sites in addition to surface migration and heterogeneous reactions
6. Desorption of by-products after film growth
7. Diffusive transport of by-products
8. Convective transport of by-products to exhaust

The influence of the most important process parameters is discussed in more detail in the following.

Total Pressure

Graphene synthesis in hot wall CVD reactors has been performed at low pressure ranges and atmospheric pressure. LPCVD was found to result in rapid growth of monolayer graphene on transition metals. Graphene growth occurs as long as there is bare substrate surface and successive layers can form beneath the existing graphene, after full coverage further deposition is not possible. APCVD, on the other hand, produces a few layers of graphene on arbitrary substrates, allowing the nucleation of successive layers of graphene on top of previously grown layers. The resulting films exhibit regions of non-uniform thickness and high defect density. In APCVD, the mass transport of gaseous carbon species is not constant across the substrate, often resulting in few layer graphene. In LPCVD, the gas phase processes become less dominant and the kinetics at the substrate surface become more important, resulting in an improvement of the graphene quality. In addition, the morphology of the substrate surface influences the growth rate of graphene at lower pressures.

Each growth mechanism has a barrier energy that must be overcome for the mechanism to occur. The thickness of the boundary layer, the region above the surface where the gas flow is stagnant due to the laminar gas flow in the reactor, plays an important role in the growth kinetics. The hydrocarbons diffuse through the boundary layer to the substrate surface where they adsorb and decompose. The carbon species diffuse to the surface while the hydrogen species diffuse back through the boundary layer into the main gas flow. Thus, there are two regions, the surface reaction region and the mass transport region, where the diffusion processes through the boundary layer take place.

In LPCVD processes, the diffusion coefficient and therefore the growth rate is increased. The thickness of the boundary layer is greater than in APCVD processes. It has been shown that monolayer growth of graphene changes to bilayer and multilayer growth at pressures above 37.5 Torr. Interestingly, the stacking of graphene layers also changes from turbostratic stacking at reduced pressures to Bernal stacking at atmospheric pressure. To achieve monolayer growth with APCVD, the growth temperature can be raised above the melting temperature of the substrate or by highly diluting carbon in hydrogen. (2)

Hydrocarbon and Hydrogen

Molecular hydrogen is not only often used in the annealing step to remove the oxide layer on the substrate, but is also essential in the graphene growth step. When H_2 and H are dissociatively chemisorbed on the surface during the annealing step, the adsorption sites of atomic hydrogen on the substrate surface lead to dehydrogenation of carbon radicals and CH_4 . Graphene growth is achieved by the formation of active surface-bound C_yH_x . On Cu substrates, hydrogen promotes graphene nucleation by providing essential CH radicals. However, it also blocks surface sites for chemisorption and thus slows down the deposition kinetics. The effect of hydrogen annealing on the growth kinetics depends on the hydrogen solubility and diffusivity in the substrate used. Depending on the H_2 diffusion coefficient, the hydrogen can either diffuse onto the surface, reducing the active surface sites and decreasing the graphene growth rate, or recombine on the surface, increasing the active surface sites and the graphene growth rate. The diffusion of hydrogen in single crystal germanium has been experimentally determined to be $4.7 \times 10^{-5} \text{ cm}^2\text{s}^{-1}$ at $800 \text{ }^\circ\text{C}$ (6), which is closer to that of nickel with $5 \times 10^{-5} \text{ cm}^2\text{s}^{-1}$ at $900 \text{ }^\circ\text{C}$ than that of copper at $2 \times 10^{-4} \text{ cm}^2\text{s}^{-1}$ at $900 \text{ }^\circ\text{C}$ (27). It can therefore be assumed that germanium behaves similarly to nickel with respect to hydrogen annealing. This means that the active surface sites are increased as well as the graphene growth rate. In the graphene etching step during cooling of the substrate to room temperature, the purity of the hydrogen used is an important factor. Studies suggest that oxidizing impurities, rather than the hydrogen itself, are responsible for the etching effect. Therefore, there is a critical concentration of oxidizing impurities that results in a balance between etching and growth rates. The catalytic substrate used directly affects the etching behavior with the oxidizing impurities present, in addition to its influence on other properties of graphene such as structure, nucleation density, layer number, crystallinity, size distribution and growth behavior. The use of hydrogen in the annealing step to clean the surface before growth changes the surface morphology and subsequently the graphene morphology. For copper, the surface becomes smoother, but more defects are introduced, which can lead to multilayer growth of graphene. Hydrogen removes weak C-C bonds and limits the thickness of graphene in this carbon etching, at high flow rates graphene edges are selectively etched. It has been found that the shape of graphene flakes during growth depends on the hydrogen and hydrocarbon flow rates. In APCVD processes with liquid Cu substrates and CH_4 as precursor at a constant low flow rate, low H_2/CH_4 ratios lead to diffusion limited growth and dendritic shaped graphene domains, while higher H_2/CH_4 ratios lead to edge attachment limited growth and compact hexagonal domains. As the CH_4 flow rate is increased, the edges of the hexagonal flakes become positively curved and even circular flakes can be grown.

In LPCVD processes, higher hydrogen flow rates are favorable due to less surface contamination from oxygen-related functional groups and more grain growth. The CH_4 flow rate itself is also very important in the graphene growth

process. In APCVD processes, lower methane flow rates result in monolayer growth and fewer defects due to lower particle concentrations from gas reactions.

Other precursors such as acetylene (C_2H_2) have also been investigated for graphene growth by CVD. C_2H_2 has a higher pyrolysis rate than CH_4 and due to vacancy defects healing processes could result in graphene with lower defect density. The C_2H_2 flow rate also affects the domain size and the number of graphene layers grown, and lower flow rates result in lower defect densities. Liquid precursors for CVD graphene growth include propanol, methanol, and ethanol vapor, which may help reduce the growth temperature due to lower decomposition temperatures. (2)

Growth Temperature

The CVD growth temperature is one of the most important process parameters due to its influence on the chemical and physical mechanisms of nucleation and growth of graphene. These mechanisms include adsorption, adsorbate migration, and desorption. Research to so far suggests that higher growth temperatures result in smoother surfaces and therefore fewer active nucleation sites and lower nucleation densities. Surface diffusion and growth rates are also increased. CVD processes that produce continuous, uniform, crystalline and monolayer graphene with low defect density are often performed at a process temperature close to or above the melting point of the growth substrate. Explanations could be the rapid dehydrogenation rate of the precursor at elevated temperatures and the increased probability of active carbon species with sufficient energy to overcome the energy barrier to adsorb on the surface. There is a lower temperature limit below which nucleation of graphene is not achieved. (2)

Growth Substrate

The substrate used determines the graphene growth process in CVD. At the beginning of graphene growth by CVD processes, transition metals were the most commonly used substrates due to the profound knowledge already available in the literature. Crystalline and high quality graphene can be obtained using transition metal substrates with their catalytic properties. Graphene has been successfully grown on Pd, Ir, Pt, Ni, and Cu, the last two being the most common choices. Nowadays, research is also focused on liquid, dielectric, or silicon-based substrates, where the grown graphene does not need to be transferred for industrial applications. To minimize long growth times and carbide formation, nucleation sites are created with catalysts. The metalloid germanium also prevents the formation of stable carbides and has direct use in electronic applications.

To obtain large graphene domains and thus high quality graphene, the nucleation sites on the substrate surface must be controlled by modifying the surface morphology. Suitable treatments prior to graphene synthesis include hydrogen,

annealing, electropolishing, plasma or chemical etching, and thin film growth. These methods reduce the active nucleation sites by changing the native oxide thickness, grain size, surface roughness, impurity density, and other properties. Smooth surfaces contribute to the synthesis of uniform and homogeneous graphene. Surface orientation also affects the quality of the resulting graphene. (2)

CVD of Graphene on Germanium

Graphene has been successfully deposited on the main surfaces (001), (110) and (111) of germanium, but the quality of the graphene as well as the interface and morphology are different. Germanium is a suitable substrate due to its catalytic surface activity and Ge-C alloy parts, which do not mix with each other under equilibrium conditions. It is assumed that the CVD synthesis of graphene on germanium is surface-mediated and self-limited, similar to the growth on copper substrates and very different from the growth on nickel substrates. The deposition temperature is the most important factor for the alignment of graphene fragments on the surface and for their coalescence into a complete layer. However, it has been shown that slow or fast cooling rates are not a determining factor. The best graphene quality is obtained at deposition temperatures of 930 °C, which is close to the melting point of germanium at 937 °C, due to the formation of a quasi-liquid surface layer. At CVD deposition temperatures of 920 °C, the graphene quality is already degraded due to the formation of defective and wrinkled graphene layers. The elevated temperature induces a higher sublimation rate and mobility on the surface, desorption of defective fragments from the surface, and higher diffusion of carbon species. Graphene on Ge(110) surface is flat and single domain growth is possible. The success for the deposition of large scales of single crystalline monolayer graphene on Ge(110) lies in the unidirectional orientation of the seeds, which can coalesce without the formation of grain boundaries. The growth is anisotropic and graphene islands align uniaxially in the $\langle\bar{1}10\rangle$ direction. Zigzag edges of graphene go in the $\langle 001\rangle$ direction and armchair edges go in the $\langle\bar{1}10\rangle$ direction. On Ge(001) and Ge(111) graphene nucleation is isotropic, resulting in polycrystalline graphene. (7)

Studies suggest that this alignment of graphene islands is not only due to the anisotropic 2-fold symmetry of the Ge(110) surface. Atomic steps on the surface and lattice matching between atomic steps and graphene edges play a crucial role in the alignment of the islands. The attachment to the atomic steps does not depend on the direction of the atomic steps, with the armchair directions of the graphene islands almost always in the same direction. This attachment occurs via strong chemical bonds, and the islands grow in a leaf-like shape with the long axis in the fast growth direction. Pre-annealing the Ge(110) surface to reduce the atomic step density on the surface can lead to isotropic graphene nucleation and an increase in grain boundary defects. Graphene island edges near atomic steps or on terraces can be passivated with germanium or terminated with hydrogen in a CVD process, depending on the H₂ partial pressure

and temperature. It has been shown that germanium termination is preferred near atomic steps and hydrogen termination on terraces. Hydrogen passivated islands interact with the surface through weak van der Waals forces instead of strong chemical bonds, making strict alignment of the graphene islands impossible. The formation energy of the covalent bond between graphene and germanium has a minimum in the observed alignment direction, making it more favorable. (26)

Graphene growth changes the structure of the underlying Ge(110) surface to a (6×2) structure, where the quenched germanium layer at the interface forms clusters ordered in the $\langle \bar{1}12 \rangle$ direction of the bulk germanium. This is not observed on pristine Ge(110) surfaces and is stabilized by the graphene layer. Studies of hydrogen intercalation at the graphene/Ge(110) interface have shown that two different phases are present at the surface after synthesis. Either graphene on the Ge(110) surface with a (6×2) structure or graphene on H-terminated (1×1) -Ge(110). Both phases can be completely transformed into each other by hydrogen intercalation or de-intercalation. (7)

Cleaning methods for Ge(110) in the literature include sonication in acetone and isopropanol for 15 minutes and etching in H_2O for 15 minutes at $90^\circ C$. Due to the use of hydrogen, the CVD reaction chamber is always evacuated before starting the process. A successful recipe for graphene growth at atmospheric pressure included the introduction of 3.6-4.6 standard cubic centimeters per minute (sccm) CH_4 after annealing at $910^\circ C$ with 200 sccm Ar and 100 sccm H_2 . The samples were rapidly cooled in the same atmosphere and then degassed for 1-2 hours in ultra high vacuum (UHV) at $400^\circ C$. The partial pressure of CH_4 was considered too high to achieve a single crystallographic orientation of graphene, and instead two rotational domains misaligned by 30° were obtained. (28) High quality graphene was also achieved by another group using the same recipe and a deposition time of 6 hours. (29)

Another APCVD process that produced high quality graphene with Raman spectra showing negligible D-band intensity involved annealing Ge(011) substrates for 30-60 minutes at $910^\circ C$ in a H_2 and Ar atmosphere before growing for 9-12 hours using 200 sccm Ar, 100 sccm H_2 , and 4.6 sccm CH_4 . These conditions allow near equilibrium growth due to the slow growth rate and high H_2/CH_4 flux ratio, suppressing defect formation and yielding relatively pristine graphene. The resulting surface was relatively flat, with hundreds of nanometer-wide flat terraces separated by atomic steps. (30)

Negligible D-band intensities were also obtained with another APCVD process where the chamber was filled with 200 sccm of argon and hydrogen after evacuation, then used H_2 gas flow rates of 27 or 30 sccm and heated to $910^\circ C$ in 30 minutes before introducing 0.5 sccm of methane for 60 to 200 minutes and cooling to room temperature under H_2 and Ar flow. (26)

In the low pressure regime at 75 Torr, monolayer graphene was grown on Ge(110) after cleaning the substrate with multiple cycles of acetone, isopropanol, and deionized water rinses. The substrates were heated to 910, 920, and $930^\circ C$ with a multi-step temperature ramp and held there for a 5 minute anneal with 200 sccm H_2 and 800 sccm Ar. The growth step was performed with an

additional 2 sccm CH₄ for 60 minutes and for cooling to room temperature a H₂ and Ar atmosphere was used again. The obtained graphene quality clearly increased with the deposition temperature used. (31)

Wafer-scale growth of single-crystal monolayer graphene has been achieved on H-terminated Ge(110), with the substrate being reusable for multiple times of high-quality graphene growth. The germanium wafer was cleaned by the standard RCA method and treated with oxygen plasma to remove organic residues. To remove the native oxide and H-terminate the germanium surface, the wafer was dipped in 10% diluted HF. In an LPCVD process, a fresh epitaxial Ge layer was deposited prior to graphene synthesis at 100 Torr with CH₄ gas diluted to 1-2% in H₂ gas at temperatures of 900-930 °C and deposition times of 5-120 minutes. After growth, the substrate was rapidly cooled to room temperature under vacuum conditions. (32)

2.2.2 PECVD of Graphene

PECVD processes provide the ability to lower the growth temperature of graphene, increase the growth rate, control and pattern the nanostructure, and produce ordered materials. The plasma-generated species dissociate the gaseous carbon source at lower temperatures than thermal dissociation, further lowering the energy barrier for graphene nucleation and growth. Another advantage is the ability to use dielectric materials as growth substrates instead of catalytic metals, eliminating graphene transfer and associated structural defects and impurities. CVD setups that combine RF plasma and hot filament heating of the reaction chamber have achieved ordered structure and low defect density graphene growth without an annealing step, due to the increase in grain size and decrease in grain boundary formation caused by the additional heat from the hot filaments. Inductively coupled RF PECVD systems produce a large plasma volume with high energy density, resulting in high graphene growth rates. Graphene has been deposited at reduced temperatures in the time frame of seconds or minutes. As growth time and plasma power are increased, atomic H etching is also increased, which can be essential for achieving monolayer growth. (2)

PECVD of Graphene on Germanium

The growth of graphene using PECVD methods is generally more novel than thermal CVD methods, so there is less literature available. However, one group has attempted to deposit graphene on Ge(110) and Ge(100) using thermal and plasma enhanced CVD. The substrates were cleaned in boiling acetone and ethyl alcohol for 2 minutes, then rinsed with isopropyl alcohol and blown dry with nitrogen. The fixed deposition parameters were a chamber pressure of 3 Torr and a deposition temperature of 757 °C. CH₄ Gas flow rates were varied between 3 and 100 sccm and the plasma atmosphere was realized with argon or hydrogen flow. The plasma used was a pulsed DC plasma with a pulse

frequency of 10 kHz and 1 μ s reverse time, and its power was varied between 40 and 100 W. In addition, a Ni foil was folded into an inverted cup and used as a Faraday cage to shield the electric field between the substrate and the plasma sheath. The best result for PECVD grown graphene on Ge(110) was achieved with 100 sccm of CH₄ and 200 sccm of Ar flowing for 8 hours at a plasma power of 40 W. This is the lowest temperature to synthesize graphene on germanium so far. However, a complete film was not formed, but monolayer graphene flakes surrounded by a defective carbon film. Interestingly, tensile strained graphene was observed when deposited via PECVD, as thermal CVD grown graphene was found to be compressively strained and p-doped, in agreement with most of the literature. The compressive strain was explained by the difference in thermal expansion coefficients. Germanium has a coefficient of thermal expansion of $5.75 \times 10^{-6} \text{K}^{-1}$ and that of graphene is $-6 \times 10^{-6} \text{K}^{-1}$. Therefore, the germanium lattice contracts during cooling, causing compression of the carbon lattice. The PECVD grown samples varied in doping and strain characteristics, which could imply variations in defect formation and long-range order across the sample. The defective carbon film around and under the crystalline flakes weakens the interaction between the germanium surface and the graphene. The graphene regions expand during cooling and could saturate existing dangling bonds by forming bonds with the now closer defective carbon layer. The tensile strain in the graphene regions could therefore be due to the attractive forces between them and the defective regions.

(33)

PECVD methods have also been used to grow vertically aligned graphene nanosheet arrays (VAGNAs) on Ge(111). VAGNAs are two-dimensional graphene nanosheets grown perpendicular to the surface of a substrate to form a three-dimensional interconnected and ordered array structure. They have potential applications in various interesting fields due to their properties such as enhanced electrochemical activity, abundant edges, large surface area, very good conductivity and open channels. The direct growth of uniform, large-area VAGNAs with a height of 30-190 nm was achieved using RF plasma on Ge(111). The substrates were cleaned with acetone, isopropanol, and deionized water before being heated in the PECVD chamber to 625 °C at a H₂ flow rate of 20 sccm. In the deposition step, plasma with a power of 20-80 W was ignited with 40 sccm CH₄, 60 sccm H₂ and 400 sccm Ar for 90 minutes. Pressure was held constant at 400 mTorr. During cooling to 250 °C, 1000 sccm of Ar and 20 sccm of H₂ flowed. (34)

RF plasma has also been used to grow graphene nanowalls on various substrates such as germanium. They are vertically oriented on a substrate and consist of a network of graphitic sheets. The nanosheets consist of 1-10 layers of graphene and are grown in a tubular RF-PECVD system. Deposition was performed at a temperature of 750 °C, a base pressure of 375 mTorr, a gas mixture of 33.3% CH₄ in H₂, and plasma powers of 50-500 W over a duration of 5-30 min. The obtained graphene nanowalls showed polycrystalline structure and consisted of few-layer graphene nanosheets, demonstrating that PECVD techniques can be used to grow high-quality graphene nanowalls on various

substrates. (35)

MW plasma has also been used to synthesize crystalline, high-quality, free-standing few-layer graphene on various substrates, including germanium. The resulting graphene is 4-6 atomic layers thick and several micrometers wide. The samples were heated with a 2 kW MW plasma for 20 minutes at 40 Torr with a 200 sccm H₂ flow, resulting in temperatures of 700 °C. For growth, CH₄ and H₂ were introduced into the chamber at a ratio of 1/8 and a total flow rate of 200 sccm. The deposition times ranged from 1 to 30000 s. The deposited few layer graphene was oriented perpendicular to the substrate surface. (36)

3 Characterization

This chapter provides an introduction to the most critical method used to characterize the quality of deposited thin films, as well as some basics of data analysis.

3.1 Raman Spectroscopy

Defects such as grain boundaries, impurities and vacancies determine the quality of graphene, with the first being the most critical. Raman spectroscopy is a fast, non-destructive and non-invasive tool to characterize graphene. In this spectroscopic technique, a laser is inelastically scattered by the sample and the Raman scattered light provides information about the structure of the sample as well as its chemistry.

The most prominent features in the Raman spectra of graphene are the G band and the 2D or G' band. The G peak at 1583 cm^{-1} appears due to bond stretching of all sp^2 atom pairs and corresponds to the E_{2g} phonon at the Brillouin center. It is a first order scattering since only one scattering event is involved. The 2D peak at 2760 cm^{-1} corresponds to second order scattering. The third peak characteristic of graphene is the D peak at 1350 cm^{-1} , which is also second order scattering. These double resonance processes occur between two non-equivalent K-points in the first Brillouin zone (BZ). When two zone-boundary phonons are connected by scattering, the 2D mode appears, while the connection of a defect and a single phonon corresponds to the D mode. Therefore, the D mode is not visible in pristine graphene without defects. (2) The intensity ratio of the D peak to the G peak I_D/I_G is used to estimate the degree of graphitization and is a measure of defect density. The intensity ratio of the 2D peak to the G peak I_{2D}/I_G and the Full Width Half Maximum (FWHM) of the 2D peak are both considered as indices of the number of graphene layers. Therefore, a low ratio of I_D/I_G and the FWHM of the 2D peak and a high ratio of I_{2D}/I_G correspond to high-quality graphene and are desirable. (37) Characteristic Raman peaks of graphene are shown in Figure 3.1.1.

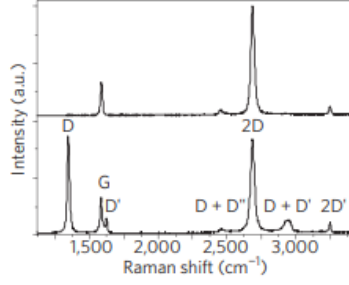


Figure 3.1.1: Raman spectra of pristine graphene (top) and defective graphene (bottom). Reprinted from (38).

The position and shape of the 2D Raman band depends on the excitation laser wavelength, drifting to higher wavenumbers at shorter wavelengths. However, its shape is also influenced by the number of graphene layers. Figure 3.1.2 shows the clear differences of the Raman peak for graphene and graphite. Not only the shape changes, but also the intensity of the G-peak to 2D-peak increases for graphite. (2)

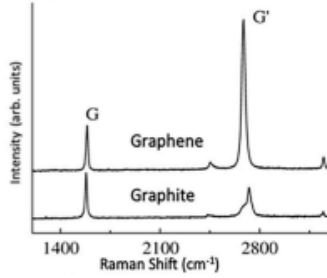


Figure 3.1.2: Raman spectra of graphene (top) and graphite (bottom). Reprinted from (2).

3.1.1 Data Analysis

The baseline correction used for the Raman spectra, which suffered greatly from luminescence, was asymmetric least squares smoothing. Asymmetric Least Squares (AsLS) is implemented in software such as Origin and is based on the Whittaker smoother. For a given vector $y = y_1, y_2, \dots, y_i$ of a signal sampled at equal intervals, there exists a smoothing series $z = z_1, z_q, \dots, z_i$ that is faithful to y . This is obtained by minimizing the penalized least squares function:

$$F = \sum_i (y_i - z_i)^2 + \lambda \sum_i (\Delta^2 z_i)^2 \tag{3.1}$$

where $\Delta^2 z_i = (z_i - z_{i-1}) - (z_{i-1} - z_{i-2}) = z_i - 2z_{i-1} + z_{i-2}$, Δ is a second order differential operator. The first term in F measures the fit to the data, and the second term is a penalty for non-smooth behavior of z . The parameter λ tunes the balance between fitness and smoothness. Then a vector w is defined to weight the fitness and the function changes to:

$$F = \sum_i w_i (y_i - z_i)^2 + \lambda \sum_i (\Delta^2 z_i)^2 \quad (3.2)$$

The minimization leads to the following system of equations:

$$(W + \lambda D^T D)z = Wy \quad (3.3)$$

where $W = \text{diag}(w)$ and D is the second order differential matrix $Dz = \Delta^2 z$. Normally, the signs of the $y - z$ residuals do not matter when a smoother is used. Therefore, a positive and a negative residual get the same weight. In the asymmetric least squares method, a parameter p is introduced to give more weight to negative residuals: $w_i = p$ if $y_i > z_i$ and $w_i = 1 - p$ otherwise. This is then transformed into an iterative application and used for baseline correction. (39) (40)

In the software OriginPro, which was used in this thesis to analyze the obtained Raman spectra, Asymmetric Least Squares Smoothing is implemented and four parameters can be changed by the user. The asymmetric factor can have a value between 0 and 1, for spectra with positive peaks a value close to 0 should be applied, in the spectra analyzed in this thesis this value was kept at 0.001. The next value is the threshold, which must also be a number between 0 and 1, the numbers used in this thesis were in the range of 0.2-0.7. The smoothing factor has a range of 2-9, this value was kept at 7. The number of iterations was also kept constant at 400. The quality of the resulting subtracted baselines was controlled by visual inspection, which is to some extent subjective.

4 Setup and Experimental Methods

This chapter explains the configuration of the experimental setup and gives a chronological description of the experiments performed.

4.1 CVD

In a first step, CVD was performed to get familiar with the system and to get a rough idea of how the different parameters will affect the graphene synthesis.

4.1.1 Experimental Setup

A sketch of the experimental setup is shown in Figure 4.1.1. The system consists of Ar, H₂, and CH₄ gas cylinders connected to mass flow controllers (MFCs) with stainless steel pipes and quarter turn valves. The Ar line is also connected to the N₂ line from the building, and the gases can be switched via a quarter turn valve. The H₂ cylinder is stored in a separate cabinet for added security. The CH₄ gas was purchased from Praxair with a purity of 99.99% and the H₂ was purchased from Linde with a purity of 99.999%. The MFCs are further connected to the tube by different pneumatic valves, the gas flow in the tube can be selected to be either left to right or right to left by opening and closing different pneumatic valves. In the experiments of this thesis, the gas flow was always selected to be from left to right. The pneumatic valves are either normally open or normally closed. To change their state, the signal from the PC goes through a programmable logic controller to the solenoids that are connected to the compressed dry air (CDA) from the building and the pneumatic valves. Check valves are connected to the tube and directly to the exhaust (not shown in the sketch for simplicity) to ensure that gas flows only in one direction and will open at a pressure of 1 PSI above atmospheric pressure to prevent overpressure in the tube. The quartz tube is 36" long and has an inside diameter of 1". Downstream, the tube is connected to two pressure gauges for different pressure ranges and directly to the exhaust with a pneumatic valve for atmospheric pressure CVD processes. For low pressure CVD processes, the tube is also connected to a throttle valve to maintain the desired pressure and a rotary vane pump. The pressure in the exhaust is slightly negative with respect to atmospheric pressure, approximately 740 Torr. All gas lines are made of stainless steel. Outside the tube is a furnace to achieve the desired temperature inside the tube. A bypass gas line is installed from the MFCs to the vacuum pump with a quarter turn valve to allow for

quick draining of the gas lines. The throttle valve and MFCs are controlled by a vacuum system controller, which is also connected to the pressure gauges. The two gauges operate in different pressure ranges to provide low and high pressure readings. The entire system is housed in a fume hood and is equipped with a hazardous gas monitor for added safety. The devices and instruments used are listed in Table 4.1.

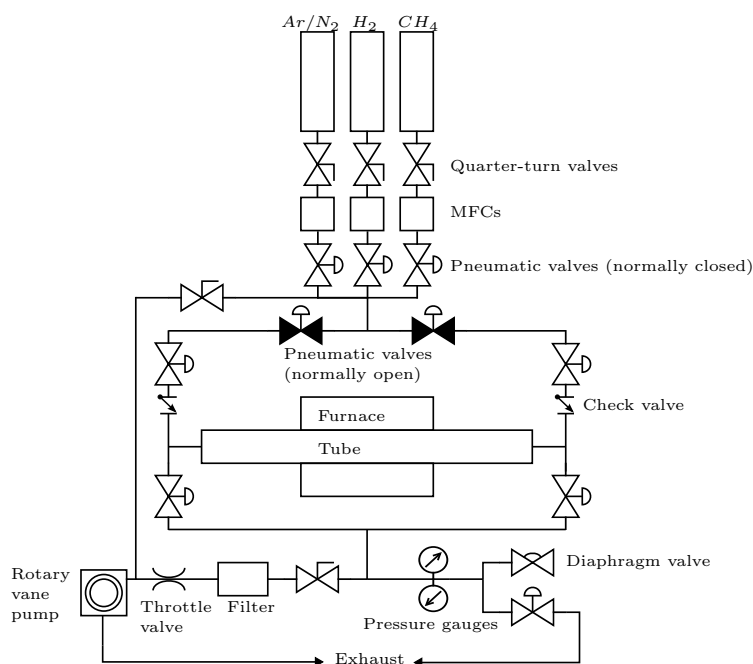


Figure 4.1.1: Schematic layout of the CVD reactor.

Table 4.1: Devices and instruments used for the experimental setup.

Device	Company	Model
Mass flow controller	MKS	GV50A series, 200 sccm range
Solenoids	Nitra Pneumatics	GM-314
Programmable logic controller		
Pneumatic valves		
Quarter turn valves		
Tube		
Furnace	Mellen	MTSC Microtherm
Controller and power supply	Mellen	PS105
PID temperature controller	Love Controls	Series 16B
Thermocouple		Type S
Vacuum System Controller	MKS	Series 946
Throttle Valve	MKS	153D
Pressure gauge	MKS	Type 722B Baratron, 10 Torr range
Pressure gauge	MKS	Type 722B Baratron, 1000 Torr range
Rotary vane pump	Edwards	RV12

4.1.2 Experimental Workflow

Sample Cleaning

The Ge(110) substrates were received as 1x1 cm² cut pieces of an undoped N-type Ge(110) wafer purchased from MTI Corporation. The substrates were first cleaned by subsequent ultrasonication for five minutes at 20 °C in acetone and isopropanol, five rinses with deionized water (DIW), and blow drying with nitrogen (N₂). This proved to be insufficient to remove the protective film residues from the polished side. In a next step, the process was repeated, but the ultrasonication duration was increased to 15 minutes. The residue was still visible even without optical magnification. Gently scraping the polished side with a micro cleanroom swab while immersed in acetone, followed by ultrasonication of the germanium again for five minutes at 20 °C in acetone and isopropanol, rinsing it five times with DIW, and blow drying it with N₂ finally resulted in a surface free of protective film, which was also confirmed by optical microscopy. As an alternative, increasing the ultrasonic time to 30 minutes was also tried because of the possibility of scratching the surface, but without satisfactory results.

The standard *ex situ* degreasing procedure became ultrasonication in acetone for five minutes, ultrasonication in isopropanol for five minutes, six DIW rinses, and then gently scraping the germanium surface with a micro-cleanroom swab in acetone, followed by ultrasonication in acetone for 15 minutes at 35 °C, ultrasonication in isopropanol for 15 minutes at 35 °C, six DIW rinses, and blow-drying with N₂.

For the *in situ* cleaning method, annealing in hydrogen was tried first because of its compatibility with the experimental process. During the naturally required heating step of the system, 20 sccm H₂ and 180 sccm Ar were introduced instead of 200 sccm Ar. Depending on the experiment performed, the desired heating temperature, heating time and pressure changed, which is a disadvantage as a cleaning method. However, completely separating the hydrogen annealing from the rest of the experimental plan would have been very impractical.

Since the produced samples showed etch marks, a hydrogen anneal without subsequent growth step was performed. The germanium sample was heated to 800 °C in 30 minutes with 180 sccm Ar and 20 sccm H₂ at 800 mTorr. The sample was then cooled to 500 °C with 200 sccm Ar and from there to room temperature without gas flow, confirming the suspicion that the H₂ was responsible for etching the surface. In a next step, hydrogen annealing was performed at 900 °C for 30 minutes (heating time 18 minutes with a heating ramp of 50 °C/minute) with 100 sccm H₂ at 75 Torr. Thus, the annealing step was somewhat separated from the heating step, as the hydrogen was not only introduced during the heating period, but also for an additional 30 minutes at constant temperature. This was repeated with an additional *ex situ* cleaning step of two minutes in the Ossila UV Ozone Cleaner. The additional *ex situ* ozone cleaning step became a standard cleaning method with a duration of 10

minutes for the samples after the degreasing cleaning step.

Hydrogen annealing was tried with several different parameters. The annealing step always took 30 minutes, but it was done at 800 °C with 100 sccm H₂ at 10 Torr, then with 150 sccm H₂ at 100 Torr, and then also at 150 Torr. In the end, the constant parameters for the H₂ anneal were a gas flow of 200 sccm H₂, a pressure of 150 Torr, and a duration of 30 minutes. The temperature still depended on the experiment, but in most cases was 800 °C with a heating time of 16 minutes.

The success of the cleaning processes was recorded by optical microscopy. The microscope used was an Olympus BX60 system microscope.

CVD

After installing the tube, a bake of the tube and sample boat was performed. The tube was completely evacuated and a leak check was performed before the tube was filled back to atmospheric pressure with N₂. A gas flow of 200 sccm N₂ and 100 sccm H₂ was maintained while the furnace was heated to 850 °C in 17 minutes and held for 30 minutes. After using H₂ gas, the system and pipes were always drained and flushed three times with N₂.

The sample cleaning steps were still evolving, the Ge(110) samples used in the CVD experiments were cleaned by several rounds of ultrasonication and scraping with a micro cleanroom swab in acetone as described at the beginning of section 4.1.2. For each experiment, a sample was placed approximately in the center of the sample boat and then in the center of the furnace to ensure a constant temperature profile. Eight experiments were performed, the parameters used in the graphene growth step are listed in Table 4.2. Before starting each experiment, the system was evacuated and a leak check was performed. For the heating step to the desired temperature of the growing step, the heating time was varied. To reach 800 °C, 30 minutes were programmed, for 700 °C, 26 minutes, and for 600 °C, 23 minutes. During heating, gas flows of 20 sccm H₂ and 180 sccm Ar were introduced into the tube. After the growth step, the gas flow was changed to 200 sccm N₂ until a temperature of 500 °C was reached. The pressure was kept constant at 800 mTorr all the time. Below 500 °C, the H₂ and CH₄ lines were drained and the system was flushed three times with N₂. After the last purging, the system was held at atmospheric pressure and cooling continued without gas flow. At 400 °C the furnace was opened to introduce a faster cooling rate. The change in gas flow was made gradually to avoid abrupt changes. More experiments were planned with other variations of H₂/CH₄ ratios than those shown in Table 4.2, but the main purpose of this series was to get familiar with the system before starting PECVD experiments. The required deposition parameters can be very different for CVD and PECVD due to the different processes involved. For time reasons it was decided that this series was sufficient.

Table 4.2: Parameters during the CVD graphene deposition step.

Temperature ($^{\circ}\text{C}$)	Pressure (mTorr)	CH_4 (sccm)	H_2 (sccm)	Time (min)
800	800	200	0	60
800	800	100	100	60
800	800	5	195	60
700	800	200	0	60
700	800	5	195	60
600	800	200	0	60
600	800	100	100	60
600	800	5	195	60

The samples produced were analyzed by optical microscopy using the Olympus BX60 system microscope and by Raman spectroscopy using the Renishaw inVia confocal microscope system. A 488 nm laser, 3000 l/mm grating and 50x magnification were used for Raman measurements. The spectra were recorded with a laser power of 60% in the range of 1000 cm^{-1} to 3300 cm^{-1} with an acquisition time of 10 seconds and 5 accumulations. Before the measurements the system was calibrated with the 520.5 cm^{-1} peak of a Si sample and the laser was focused on the surface. If graphene was deposited and therefore a 2D band was visible in the Raman spectra, the laser was focused to maximize the 2D band, which may be different from focusing on the surface. However, this process was also somewhat subjective. The laser power was chosen to be as low as possible while still being able to clearly distinguish Raman features from noise. For each sample, Raman spectra were recorded at approximately the center and near the four edges of the sample.

4.2 PECVD

4.2.1 Experimental Setup

To perform PECVD processes, the experimental setup was set up as shown in Figure 4.2.1. The LFRF-501 RF plasma generator from SMI Technology is an industrial spark tester consisting of a single wound Tesla coil wound on a thermo-plastic cone and ruggedly mounted in an insulated enclosure. High quality mica capacitors and a sturdy 4 point adjustable tungsten gap are also used. The generator is connected to a copper foil with a RF power transmission cable, the RF current is adjustable from 10 mA to 250 mA and the output voltage is in the order of 50 kV at 2 MHz. The high frequency spark is adjustable from 1/16" to 2". The operating pressure is in the range of mTorr to dTorr, depending on the gas type and flow rate. The copper foil was cut into a 3.8 cm wide piece and wrapped around the quartz tube 11.8 cm to the right of the left bearing that held the quartz tube in place in the system. The furnace was placed with a distance of 7.9 cm between the edge of the copper foil and the edge of the furnace.

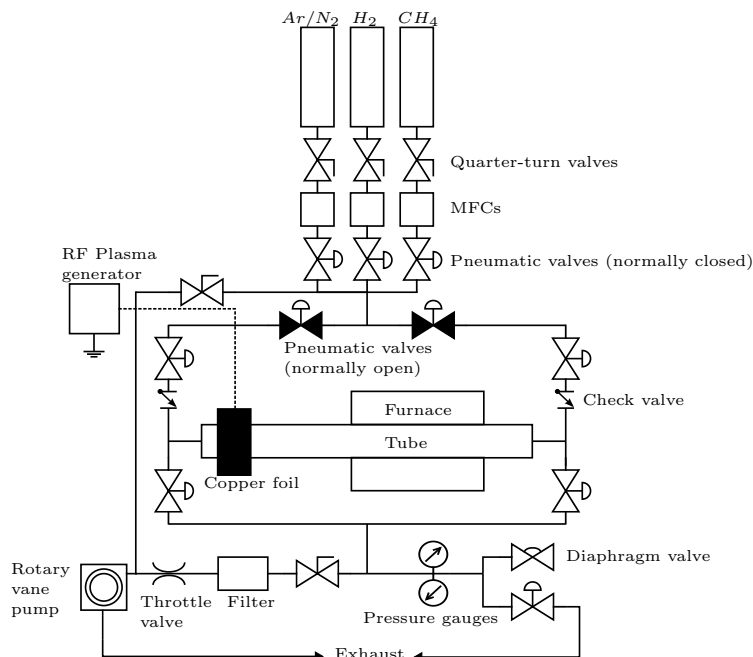


Figure 4.2.1: Schematic layout of the PECVD reactor. The dashed line indicates a RF power transmission cable.

4.2.2 Experimental Workflow

The samples were still cleaned as before, unless otherwise specified, and the positioning of the sample in the boat and the furnace remained the same, see section 4.1.2. Four PECVD experiments were performed.

First, an experimental procedure from the CVD experiments was attempted to be reproduced with plasma ignited during the deposition step, including the same steps after deposition. The sample was heated to 800 °C in 30 minutes with 180 sccm Ar and 20 sccm H₂ flowing. During the 60 minute deposition step the gas flow was changed to 200 sccm CH₄. The pressure was kept constant at 800 mTorr. However, the plasma was not stable and the generator settings, such as the high frequency spark and the high frequency current, were readjusted and changed frequently. It was concluded that the pressure was too high to form a stable plasma. Experiments without samples showed that the plasma was stable for at least 10 minutes with a flow of 20 sccm Ar at a pressure of 150 mTorr and a gas flow of 25 sccm CH₄ at a pressure of 100 mTorr. Lower pressures were not possible with the installed pumping system.

The next sample was heated to 800 °C with 25 sccm H₂ flowing at a pressure of 100 mTorr. During the 60 minute deposition step, the throttle valve was left fully open to achieve the lowest possible pressure. However, the pressure was not constant during the experiment and this makes the experiment not reproducible. Both a flow rate of 20 sccm and 25 sccm CH₄ were tried and the pressure ranged from 100 mTorr to 170 mTorr. Again, the plasma was not stable and had to be constantly readjusted. The sample was then cooled to

500 °C with 25 sccm N₂. The rest of the procedure was the same as before and the plasma did not improve.

Another experiment with the throttle open all the time was done with 25 sccm CH₄ and 25 sccm H₂ during the growing step. The pressure was in the order of 80 mTorr during the heating step to 800 °C in 30 minutes with a flow of 25 sccm H₂, ranged from 185 mTorr to 239 mTorr during the deposition step, and was in the range of 113 mTorr during the cooling step to 500 °C with a flow of 25 sccm N₂. Again, the plasma was not stable.

The final sample was cleaned using the standard degreasing procedure described in section 4.1.2. The substrate was heated to 900 °C in 34 minutes under a flow of 20 sccm H₂ and 30 sccm Ar. During the 60 minute growth step, 20 sccm H₂, 20 sccm CH₄ and 10 sccm Ar flowed. For cooling to 500 °C, 50 sccm of Ar was used. The pressure was kept constant at 300 mTorr, which was the lowest pressure possible because of the background pressure. The plasma was still not stable.

Unstable plasma in the four experiments means that it started bright but flickered after a few minutes and soon disappeared. As the experiment progressed, it was not possible to ignite a bright plasma, and often no plasma could be ignited at all. It was concluded that the pressure required to form a stable plasma could not be achieved. The reason for this was the rotary vane pump, but also the MFCs, which probably do not produce a stable flow rate below 25 sccm and are not reliable at flow rates below 10 sccm. In addition, the tungsten points of the generator are believed to have deteriorated. However, cleaning the contacts with sandpaper and readjusting the gaps did not change the performance. Another problem with the plasma generator was the lack of a scaled setting and reading of the plasma power, which made reproducibility of this parameter difficult.

Many more experiments were planned, but not carried out because a stable plasma could not be achieved. The samples produced were again examined by optical microscopy and Raman spectroscopy, as described in section 4.1.2.

4.3 Dual Furnace CVD

4.3.1 Experimental setup

To deposit graphene on Ge(110) at deposition temperatures lower than commercial CVD methods, a method other than PECVD was focused on. Qian et al. successfully deposited graphene on copper substrates at reduced temperatures of 300 °C using a CVD process with three furnaces. The first furnace was heated to a temperature of 1000 °C, the second to 720 °C, and the third, containing the Cu substrate, to 300 °C. The high temperatures are due to the high reaction energy barrier of the decomposition of CH₄, where the conversion rate can only reach the order of 10⁻¹ at temperatures above 1000 °C. (41)

Therefore, a second Mellen furnace was installed in the CVD experimental setup with a distance of 8.5 cm between the furnaces. A schematic of the

adapted experimental setup is shown in Figure 4.3.1.

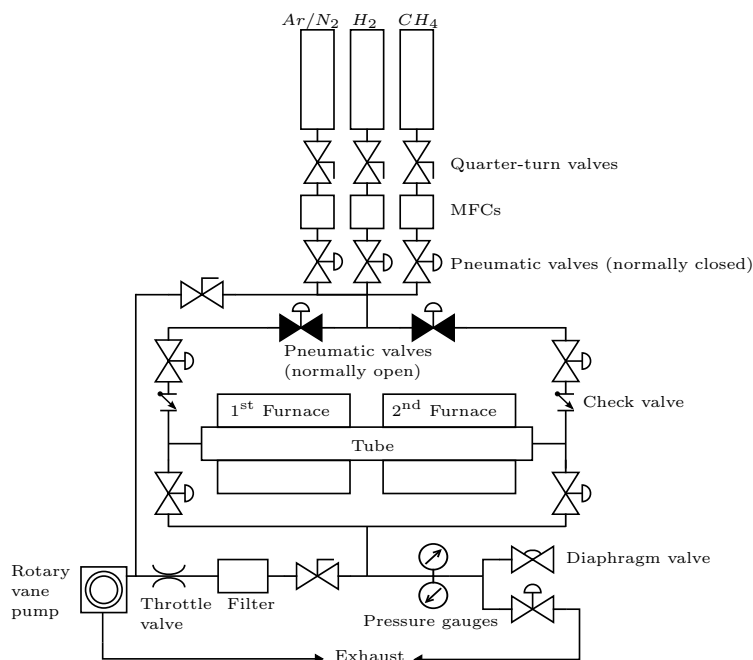


Figure 4.3.1: Schematic layout of the dual furnace CVD reactor.

4.3.2 Experimental Workflow

The Ge(110) samples were cleaned by the standard degreasing method followed by 10 minutes in the UV Ozone Cleaner. As a first step, eight experiments were performed with the parameters during the deposition step listed in Table 4.3. The first furnace was at 1000 °C and the second furnace was at 800 °C in each experiment. The samples were placed in the center of the boat and then in the center of the second furnace. The heating and annealing steps were slightly different. The system was purged with N₂ for one minute before evacuation and leak check. For the H₂:CH₄:Ar = 50:10:90 sccm sample, both furnaces were heated to deposition temperature in 30 minutes while 100 sccm of H₂ was injected into the tube at a pressure of 10 Torr. For H₂:CH₄:Ar = 100:10:40 sccm, the second furnace was heated to 800 °C in 16 minutes and held for 30 minutes, while the first furnace was heated to 1000 °C and 150 sccm of H₂ flowed at a pressure of 100 Torr. For H₂:CH₄:Ar = 10:10:130 sccm the pressure was increased to 150 Torr. After the deposition step, the CH₄ and H₂ lines were drained and the system was flushed three times with N₂. For the rest of the samples, the pressure was kept at 150 Torr during the annealing step, during cooling 150 sccm N₂ were introduced during slow cooling to room temperature or at least to 400 °C. The sample with H₂:CH₄:Ar = 200:200:200 sccm had 200 sccm H₂ flowing during annealing and 200 sccm N₂ during slow cooling. This experiment was not planned in the series, but was done out of curiosity and because a H₂/CH₄ ratio of 1 seemed to be the most successful

for graphene deposition so far.

The MFCs were otherwise used at their reliability limit of 10 sccm, because of the common literature CH_4 flow rates for graphene deposition by CVD below 10 sccm, as described in chapter 2.2.1. However, corresponding MFCs were not available.

Table 4.3: Parameters during the graphene deposition step of the first series of experiments with dual furnace CVD.

Pressure (Torr)	CH_4 (sccm)	H_2 (sccm)	Ar (sccm)	Time (min)
10	10	0	140	60
10	10	10	130	60
10	10	25	115	60
10	10	50	90	60
10	10	100	40	60
10	200	200	200	60
1	10	10	130	60
100	10	10	130	60

More experiments were planned in this series, such as further increasing the pressure, changing the growth time, and also changing the temperature of the second furnace. However, the results of this series were not as good as hoped for, and a comparison with the preliminary single furnace CVD experiments led to a new series of experiments. The samples produced were again examined by optical microscopy and Raman spectroscopy, as described in section 4.1.2.

The parameters used in the deposition step of the second experimental series are listed in Table 4.4, the growth time was always 60 minutes. All samples were cleaned with the standard degreasing method. The first experiment was reproduced from the CVD series with only one furnace as listed in Table 4.2. Therefore, the second furnace was heated to deposition temperature in 30 minutes while 20 sccm H_2 and 180 sccm Ar were flowing. The sample was slowly cooled to a temperature of 400 °C with 200 sccm of Ar flowing, then the furnace was opened.

The cleaning steps were then adjusted and the other samples were also cleaned for 10 minutes in the UV ozone cleaner. The system was flushed again with N_2 for one minute before evacuation and leak check. The second furnace was heated to deposition temperature in 16 minutes followed by a 30 minute anneal, during these steps the H_2 flow rate was set to 200 sccm and the pressure was 150 Torr. During slow cooling 200 sccm N_2 was introduced. In the other experiments, the first furnace either followed the same program as the second furnace or was heated to 1000 °C in 46 minutes. The samples produced were again examined by optical microscopy and Raman spectroscopy, as described in section 4.1.2, and also using a scanning electron microscope (SEM), the FEI Quanta 3D FEG FIB.

Table 4.4: Parameters during the graphene deposition step of the second series of experiments using dual furnace CVD.

Temperature 1 st (°C)	Temperature 2 nd (°C)	Pressure (mTorr)	CH ₄ (sccm)	H ₂ (sccm)
-	800	800	100	100
-	800	800	100	100
800	800	800	100	100
1000	800	800	100	100

These experiments led to the final set of experiments whose deposition parameters are listed in Table 4.5. The Ge substrates were cleaned *ex-situ* with the standard degreasing method and 10 minutes in the UV ozone cleaner. The samples were placed in the center of the sample boat and then in the center of the second furnace. Prior to evacuation and leak testing, the system was flushed with N₂ for one minute. The first furnace was always heated to 800 °C. Both furnaces ran the same program and the heating rate was set to 50 °C/minute, corresponding to the furnace with the higher temperature. The heating step was followed by a 30 minute anneal, during which the H₂ flow rate was set to 200 sccm and the pressure was 150 Torr. During the slow cooling 200 sccm N₂ was introduced. The 10 and 100 Torr experiments were repeated once each. The prepared samples were again examined by SEM and Raman spectroscopy as described in section 4.1.2.

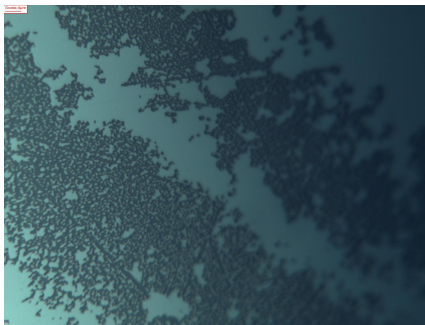
Table 4.5: Parameters during the graphene deposition step of the third series of experiments using dual furnace CVD.

Temperature 2 nd furnace(°C)	Pressure (Torr)	CH ₄ (sccm)	H ₂ (sccm)	Time (min)
800	0.8	100	100	60
800	0.8	100	100	50
800	0.8	100	100	40
800	0.8	100	100	30
800	0.8	100	100	20
800	0.8	100	100	5
800	10	100	100	60
800	100	100	100	60
800	760	100	100	60
800	0.8	10	190	40
800	0.8	60	140	40
800	0.8	140	60	40
800	0.8	190	10	40
800	0.8	200	0	40
900	0.8	100	100	40
850	0.8	100	100	40
750	0.8	100	100	40
700	0.8	100	100	40

5 Results

5.1 Sample Cleaning

Optical microscope images of the germanium substrates with visible residual protective film are shown in Figure 5.1.1a. This sample was not scraped with the micro cleanroom swab and it is concluded that ultrasonication in acetone and isopropanol is not sufficient to clean the surface. For comparison, the resulting surface from the standard degreasing method is shown in Figure 5.1.1b. Optical microscope images of the resulting surfaces from the various hydrogen annealing trials are shown in Figure 5.1.2. It is concluded that sufficiently high pressures and hydrogen flow rates are required, in addition to sufficient time for the surface to be completely etched by the H_2 and thus clean. Unfortunately, the lens for the 100x magnification in the microscope does not focus evenly over the whole area, and there was some kind of staining on the lens, which can be clearly seen in Figure 5.1.2d.



(a) Residual protective film after ultrasonication in acetone and isopropanol.

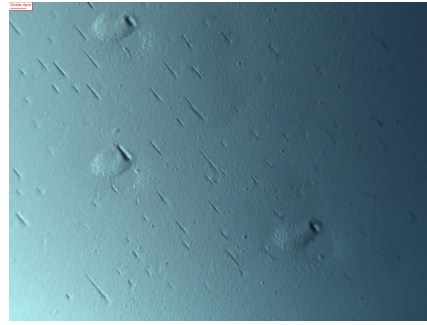


(b) Clean surface with standard degreasing methods, including micro cleanroom swabs.

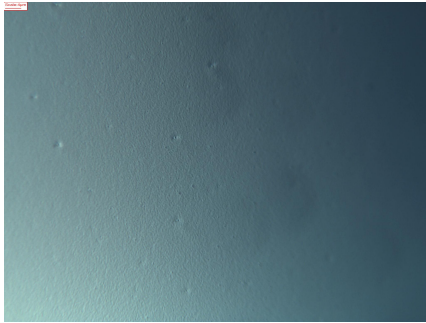
Figure 5.1.1: Optical microscope images of polished Ge(110) surface after degreasing cleaning step, 100x magnification and scale bar of 4 μm .



(a) Hydrogen annealing during the heating step, 20 sccm H₂ and 180 sccm Ar at 800 mTorr while heating to 800 °C in 30 minutes.



(b) Hydrogen anneal, 100 sccm H₂ at 75 Torr and 900 °C for 30 minutes plus 18 minute heating step.



(c) Hydrogen anneal, same procedure as 5.1.2b with additional ozone cleaning for two minutes.



(d) Hydrogen anneal, 200 sccm H₂ at 150 Torr and 800 °C for 30 minutes plus 16 minute heating step with additional ozone cleaning for ten minutes.

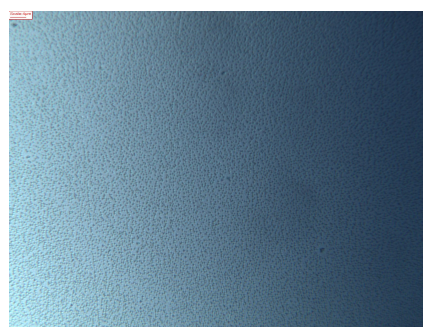
Figure 5.1.2: Optical microscope images of the polished Ge(110) surface after H₂ annealing cleaning step, 100x magnification and scale bar of 4 μm..

5.2 Single Furnace CVD

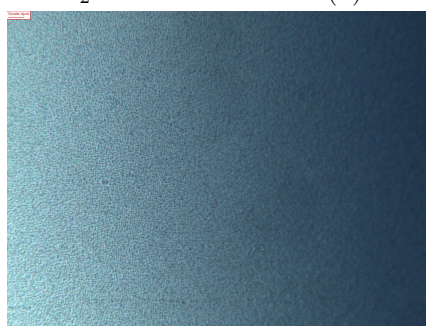
Optical microscope images of the samples with a CVD deposition temperature of 600 °C are shown in Figure 5.2.1, those with a deposition temperature of 700 °C in Figure 5.2.2, and those with a deposition temperature of 800 °C in Figure 5.2.3. The visible features are the etch marks from H₂, since the H₂ anneal was still developing and the samples did not have an additional hydrogen annealing step. Interestingly, the etch marks at 600 °C have a higher density and look like small dots, the etch pits at 700 °C are larger and appear to be deeper, but it looks like some of the etch pits have already filled due to surface diffusion. At 800 °C, long and rectangular etch pits appear with a preferred direction. It is unclear whether the preferred direction is due to surface orientation or gas flow. The etch pits also show a preferred orientation along scratches as shown in Figure 5.2.1a.



(a) 200 sccm CH₄ and 0 sccm H₂.



(b) 100 sccm CH₄ and 100 sccm H₂.

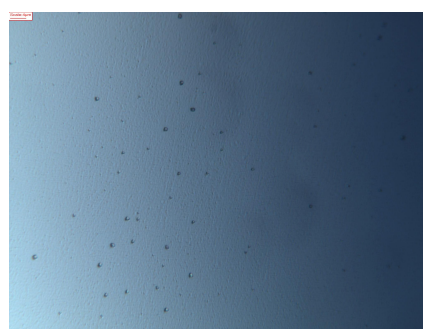


(c) 5 sccm CH₄ and 195 sccm H₂.

Figure 5.2.1: Optical microscope images of graphene on Ge(110) samples at 600 °C single furnace CVD deposition temperature, 100x magnification and 4 μm scale bar.



(a) 200 sccm CH₄ and 0 sccm H₂.



(b) 5 sccm CH₄ and 195 sccm H₂.

Figure 5.2.2: Optical microscope images of graphene on Ge(110) samples at 700 °C single furnace CVD deposition temperature, 100x magnification and 4 μm scale bar.

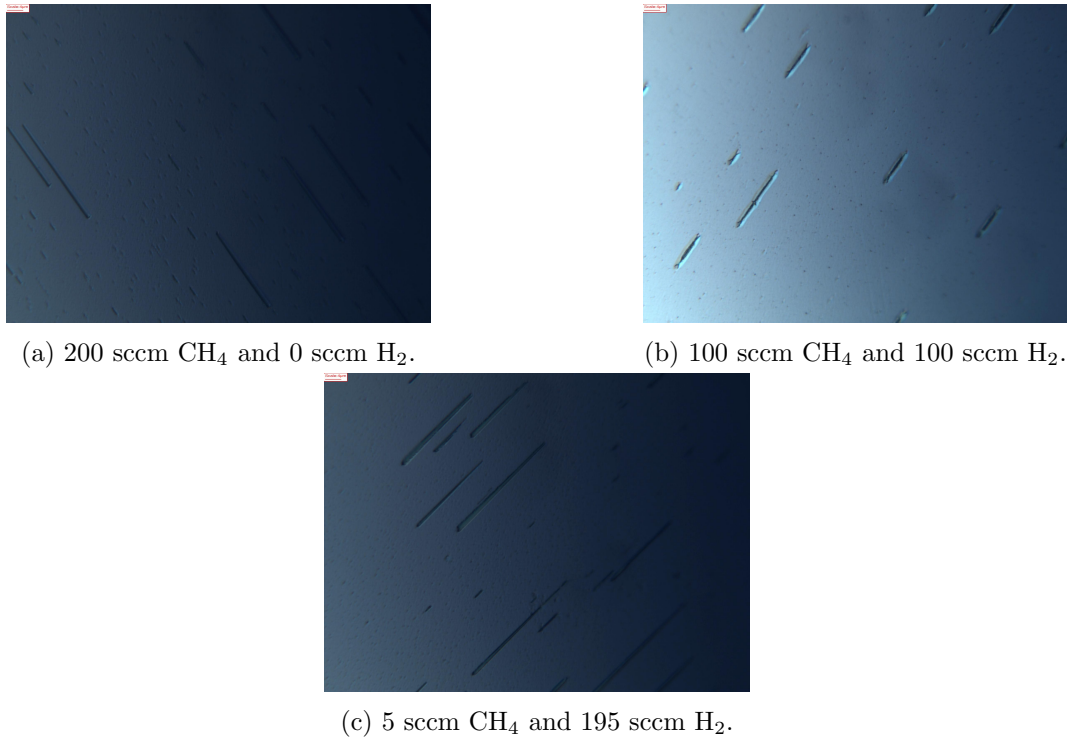


Figure 5.2.3: Optical microscope images of graphene on Ge(110) samples at 800 °C single furnace CVD deposition temperature, 100x magnification and 4 μm scale bar.

The Raman spectra of the samples grown by single furnace CVD at 600 °C are shown in Figure 5.2.4, those grown at 700 °C in Figure 5.2.5, and those grown at 800 °C in Figures 5.2.6 and 5.2.7, respectively. For all samples grown at 700 °C and 800 °C, the spectra were recorded five times with the laser spot focused on an etch pit and on the intact surface. This was not possible for the 600 °C samples due to the high density of etch pits. The spectra of the five measurement points on each sample were averaged to obtain a better signal-to-noise ratio, and the luminescence background was subtracted using the asymmetric least square method described in chapter 3.1.1. Then the spectra were normalized between 0 and 1. The maximum value of the standard deviation (STD) was divided by the maximum value of the corresponding five recorded spectra to get some information about the homogeneity of the samples. This maximum relative standard deviation is listed together with the background subtraction parameters in Tables 5.1, 5.2, 5.3, 5.4 and 5.5. The data analysis software used was OriginPro.

The D peak at $\sim 1360\text{ cm}^{-1}$ and the G peak at $\sim 1600\text{ cm}^{-1}$ are visible in all spectra. The 2D peak at $\sim 2700\text{ cm}^{-1}$, which is the most characteristic graphene Raman peak, is only clearly visible in the sample grown at 800 °C with 100 sccm CH₄ and 100 sccm H₂ when the laser is focused on the etch pits. The relative standard deviation of the averaged spectra is larger when the laser is focused on the etch pits during the Raman measurements. In the case of

this sample with successful graphene deposition, the difference between the five spectra recorded at different sample spots is particularly large, as shown in Figure 5.2.7a. Therefore, the spectrum with the lowest I_D/I_G ratio and FWHM of the 2D peak and the highest I_{2D}/I_G ratio was selected and the peaks were fitted with a Lorentz function

$y = y_0 + \frac{2 \times A}{\pi} \times \frac{w}{4 \times (x - x_c)^2 + w^2}$, where y_0 is the offset, A is the area, w is the FWHM, and x_c is the center of the peak. The derived parameter is the height of the peak H with $H = \frac{2 \times A}{\pi \times w}$. The fitting parameters with their standard errors are listed in Table 5.6. Using the peak height derived from the fit parameters, the I_D/I_G ratio was calculated to be 1.860 ± 0.017 and the I_{2D}/I_G ratio was calculated to be 0.333 ± 0.007 . Uncertainty estimates were calculated using the standard errors of the parameters and the propagation of uncorrelated uncertainty. The spectrum indicates successful deposition of graphene with many defects. However, the spectrum also indicates that it might not be monolayer graphene. The H_2 etching probably created active surface sites that facilitated graphene formation. On all other Ge(110) samples, amorphous carbon, graphite, highly defective graphene, or a mixture of these appears to have been deposited instead of graphene. The G band is characteristic of sp^2 hybridized carbon materials, indicating the presence of a hexagonal carbon lattice as in graphitic or graphene-like structures. The D band corresponds to defects and disorder in the carbon lattice and is due to sp^3 hybridized carbon atoms or localized states in the carbon network. The deposited material is likely to have a high degree of disorder or structural changes.

Furthermore, the sharp features at $\sim 1550 \text{ cm}^{-1}$ and at $\sim 2330 \text{ cm}^{-1}$ correspond to oxygen and nitrogen from the environment, respectively. (7)

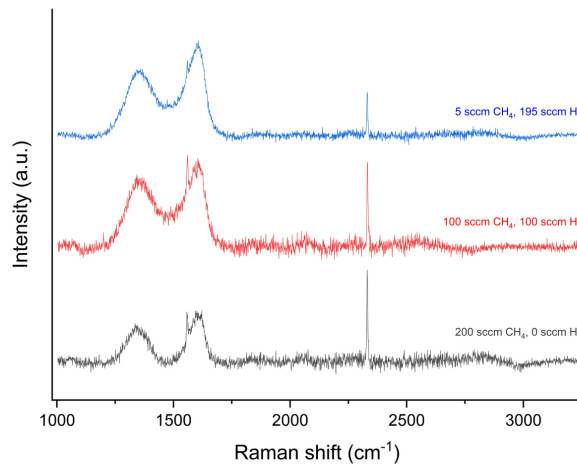
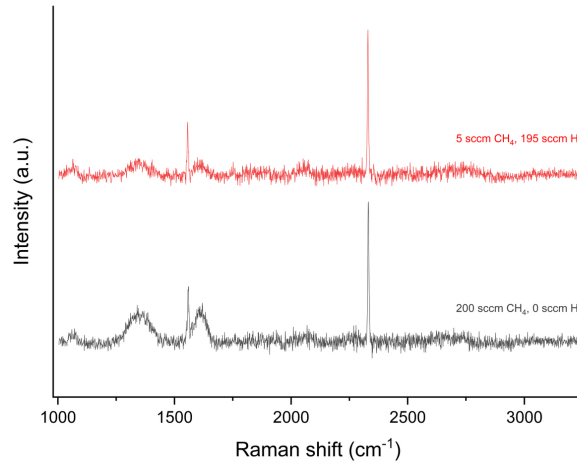


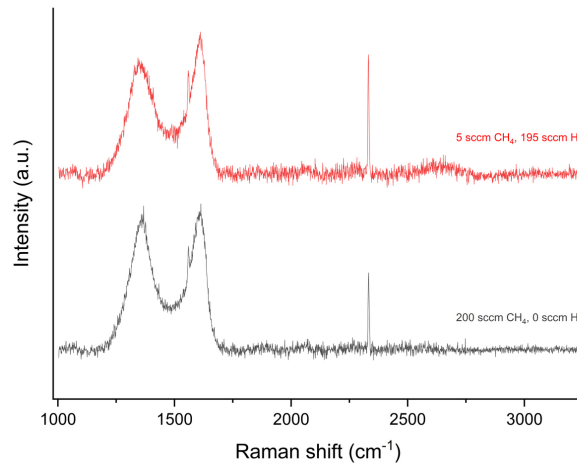
Figure 5.2.4: Averaged Raman spectra of graphene on Ge(110) samples at 600 °C single furnace CVD deposition temperature.

Table 5.1: Background subtraction parameters asymmetric factor, threshold, smoothing factor, and number of iterations for the asymmetric least squares method and relative standard deviation for the Raman spectra of graphene on Ge(110) samples with 600 °C single furnace CVD deposition temperature.

CH ₄ (sccm)	H ₂ (sccm)	As. factor	Threshold	Smooth. factor	Iterations	Relative STD
200	0	0.001	0.07	7	400	19%
100	100	0.001	0.06	7	400	11%
5	195	0.001	0.05	7	400	20%



(a) Intact surface.



(b) Etch pits.

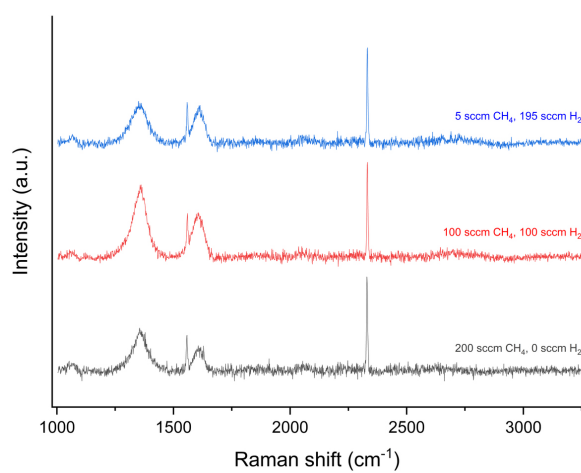
Figure 5.2.5: Averaged Raman spectra of graphene on Ge(110) samples at 700 °C single furnace CVD deposition temperature.

Table 5.2: Background subtraction parameters asymmetric factor, threshold, smoothing factor, and number of iterations for the asymmetric least squares method and relative standard deviation for the Raman spectra of graphene on Ge(110) samples with 700 °C single furnace CVD deposition temperature, intact surface.

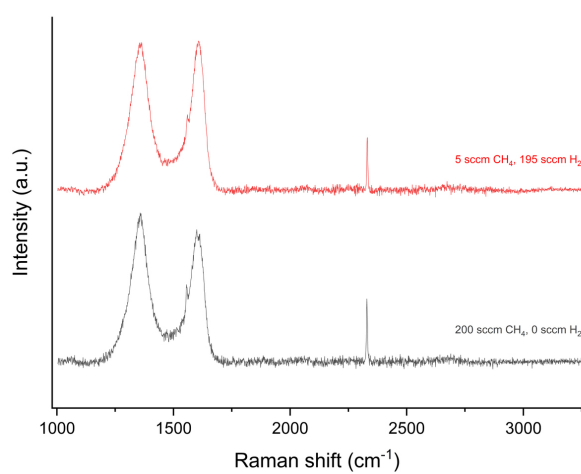
CH ₄ (sccm)	H ₂ (sccm)	As. factor	Threshold	Smooth. factor	Iterations	Relative STD
200	0	0.001	0.05	7	400	7%
5	195	0.001	0.04	7	400	10%

Table 5.3: Background subtraction parameters asymmetric factor, threshold, smoothing factor, and number of iterations for the asymmetric least squares method and relative standard deviation for the Raman spectra of graphene on Ge(110) samples with 700 °C single furnace CVD deposition temperature, etch pits.

CH ₄ (sccm)	H ₂ (sccm)	As. factor	Threshold	Smooth. factor	Iterations	Relative STD
200	0	0.001	0.04	7	400	30%
5	195	0.001	0.04	7	400	20%

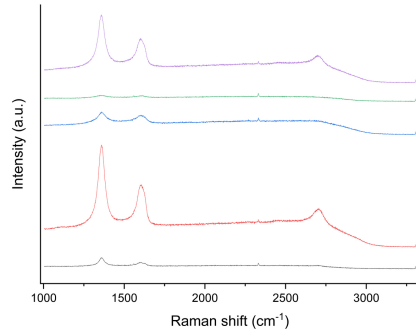


(a) Intact surface.

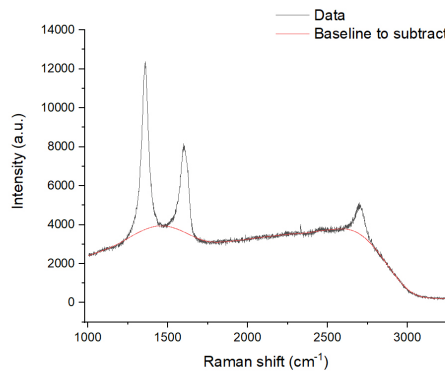


(b) Etch pits.

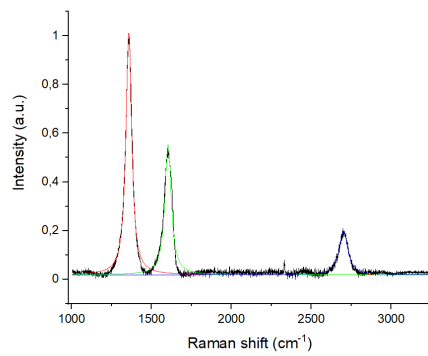
Figure 5.2.6: Averaged Raman spectra of graphene on Ge(110) samples at 800 °C single furnace CVD deposition temperature.



(a) Five spectra recorded at different etch pits.



(b) Raw data (black) with background for subtraction (red) of the uppermost spectra (violet) in the Figure 5.2.7a.



(c) Background corrected spectra (result of Figure 5.2.7b) with fitted Lorentz peaks.

Figure 5.2.7: Raman spectra of graphene on Ge(110) samples at 800 °C single furnace CVD deposition temperature and 100 sccm CH₄ and 100 sccm H₂, focused on the etch pits.

Table 5.4: Background subtraction parameters asymmetric factor, threshold, smoothing factor, and number of iterations for the asymmetric least squares method and relative standard deviation for the averaged Raman spectra of graphene on Ge(110) samples with 800 °C single furnace CVD deposition temperature, intact surface.

CH ₄ (sccm)	H ₂ (sccm)	As. factor	Threshold	Smooth. factor	Iterations	Relative STD
200	0	0.001	0.04	7	400	8%
100	100	0.001	0.04	7	400	14%
5	195	0.001	0.04	7	400	6%

Table 5.5: Background subtraction parameters asymmetric factor, threshold, smoothing factor, and number of iterations for the asymmetric least squares method and relative standard deviation for the Raman spectra of graphene on Ge(110) samples with 800 °C single furnace CVD deposition temperature, etch pits

CH ₄ (sccm)	H ₂ (sccm)	As. factor	Threshold	Smooth. factor	Iterations	Relative STD
200	0	0.001	0.03	7	400	30%
100	100	0.001	0.02	7	400	50%
5	195	0.001	0.03	7	400	30%

Table 5.6: Lorentz function fit parameters y-offset, peak center, area, FWHM and derived peak height with their standard errors for the fitted peaks in Figure 5.2.7c.

Peak	y_0	x_c	w	A	H
D	0.0185 ± 0.0005	1357.58 ± 0.09	43.0 ± 0.3	67.1 ± 0.3	0.993 ± 0.005
G	0.0185 ± 0.0005	1603.31 ± 0.18	48.3 ± 0.5	40.5 ± 0.4	0.534 ± 0.004
2D	0.0185 ± 0.0005	2702.2 ± 0.6	64.1 ± 1.6	18.0 ± 0.4	0.178 ± 0.003

5.3 PECVD

The optical microscope images of the samples with a deposition temperature of 800 °C are shown in Figure 5.3.1 and the sample with 900 °C in Figure 5.3.2. Interestingly, the etch pits are very different in shape and density. Temperature and H₂ flow rate are not the only parameters influencing the resulting surface, but apparently pressure and total flow rate as well. However, a sample underwent the same treatment with PECVD, shown in Figure 5.3.1a, and CVD, shown in Figure 5.2.3a, and the resulting surfaces are different. The PECVD sample looks like many of the etch pits have already been refilled, but it is unclear why this was possible for this particular sample. Even more interesting is the difference in etch pits between the sample in Figure 5.3.1b and the sample in Figure 5.3.1c, since both experienced the same temperature, duration, and H₂ flow during the heating step, and the pressure was also similar. The degreasing steps before the experiments were also performed in the same way. However, the sample in Figure 5.3.1b looks similar to the samples that were subjected to a temperature of 700 °C in the CVD series, see Figure 5.2.2. Faint rectangular etch pits connecting deeper and circular etch pits may indicate how the deep rectangular etch pits develop. The etch pits on the sample surface in Figure 5.3.1c look smaller but similar to those on the sample surface in Figure 5.3.2, although they experienced a different temperature, duration, and pressure during heating. The H₂ flow rate was similar, but the total flow rate was different. In addition, the degreasing steps were not performed in the same manner. It is possible that the plasma also altered the surface significantly.

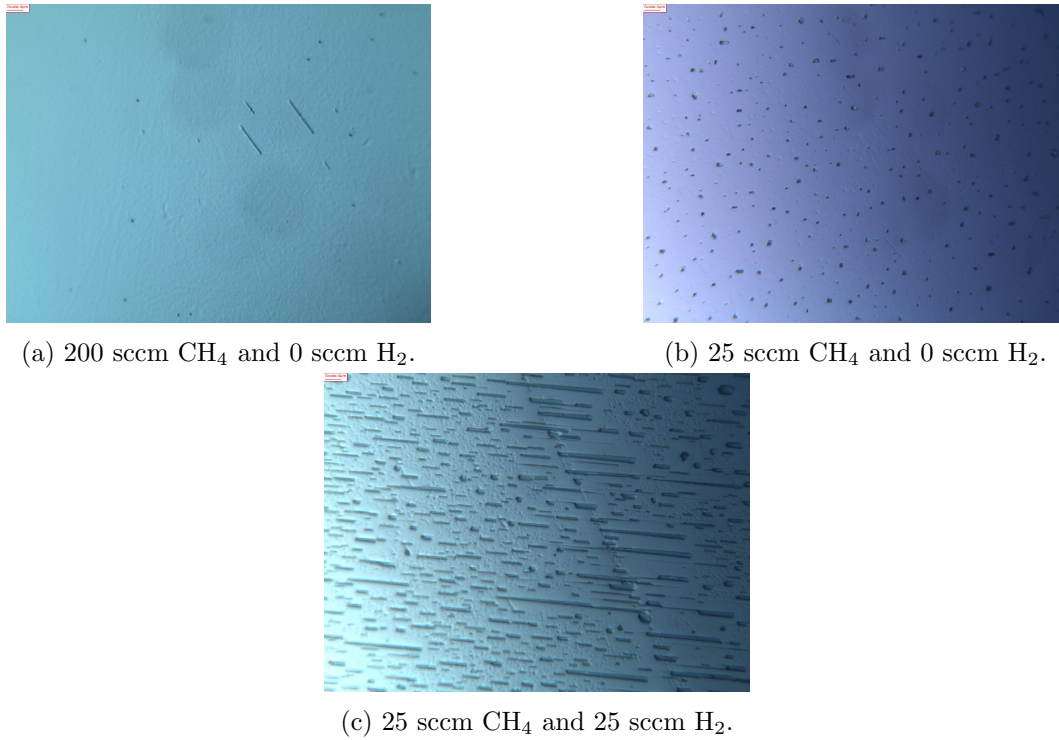


Figure 5.3.1: Optical microscope images of graphene on Ge(110) samples at 800 °C PECVD deposition temperature, 100x magnification, and 4 μm scale bar.

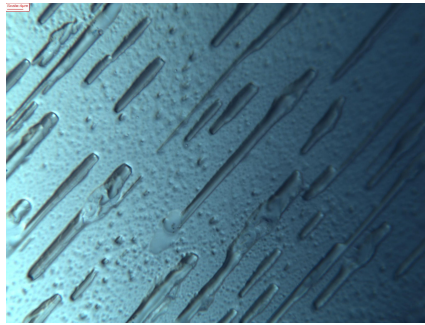
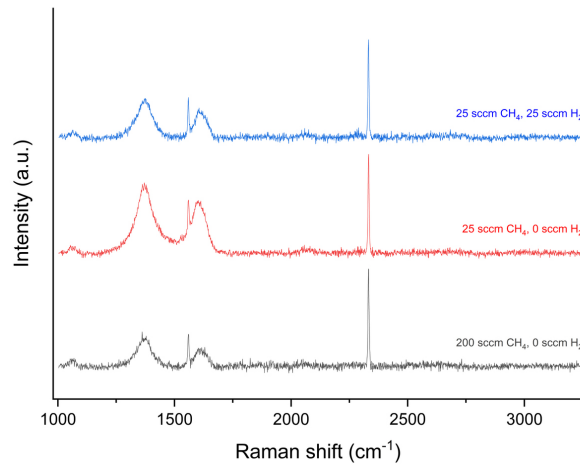


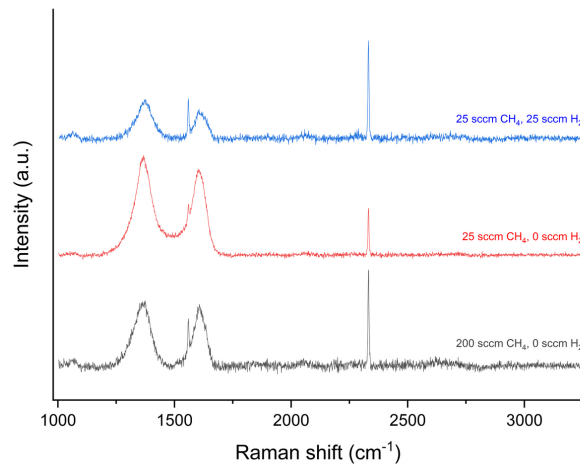
Figure 5.3.2: Optical microscope images of graphene on Ge(110) sample at 900 °C PECVD deposition temperature and 20 sccm CH₄, 20 sccm H₂ and 10 sccm Ar, 100x magnification and scale bar of 4 μm .

The averaged Raman spectra of the samples produced in the PECVD experiment series are shown in Figures 5.3.3 and 5.3.4. The Raman measurements were again performed with the laser spot focused on the etch pits and on the intact surface. The measurement and analysis were performed in the same way as for the CVD series, see section 5.2. The relative standard deviation of the averaged spectra together with the background subtraction parameters are

given in Tables 5.7 and 5.8. In all spectra the D and G peaks are visible again, as well as the ambient oxygen and nitrogen peaks. A mixture of amorphous carbon, graphite and highly defective graphene has probably been deposited on the samples again. The faint hint of a 2D peak in the Raman spectra of the sample with a deposition temperature of 900 °C, shown in Figure 5.3.4, is probably due to artifacts from the subtraction of the luminescent background, but it could be that graphene was deposited on these samples. Furthermore, a D' peak may be visible at slightly higher wavenumbers than the G peak.



(a) Intact surface.



(b) Etch pits.

Figure 5.3.3: Averaged Raman spectra of graphene on Ge(110) samples at 800 °C PECVD deposition temperature.

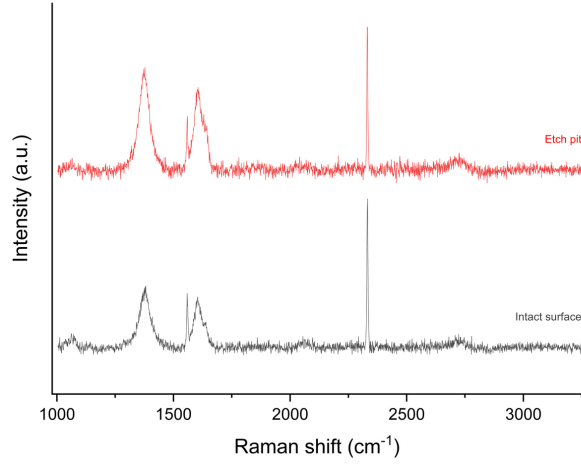


Figure 5.3.4: Averaged Raman spectra of graphene on Ge(110) samples with 900 °C PECVD deposition temperature and 20 sccm CH₄, 20 sccm H₂ and 10 sccm Ar.

Table 5.7: Background subtraction parameters asymmetric factor, threshold, smoothing factor and number of iterations for the asymmetric least square method and relative standard deviation for the averaged Raman spectra of graphene on Ge(110) samples with 800 °C and 900 °C PECVD deposition temperature, intact surface.

CH ₄ (sccm)	H ₂ (sccm)	As. factor	Threshold	Smooth. factor	Iterations	Relative STD
200	0	0.001	0.03	7	400	9%
25	25	0.001	0.03	7	400	8%
25	0	0.001	0.02	7	400	7%
20	20	0.001	0.03	7	400	7%

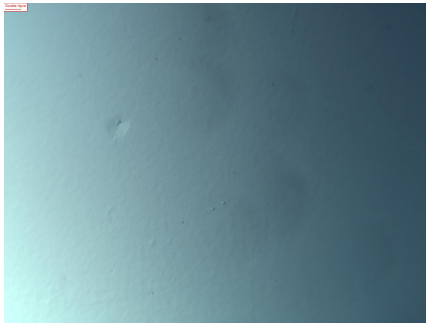
Table 5.8: Background subtraction parameters asymmetric factor, threshold, smoothing factor and number of iterations for asymmetric least square method and relative standard deviation for the averaged Raman spectra of graphene on Ge(110) samples with 800 °C and 900 °C PECVD deposition temperature, etch pits.

CH ₄ (sccm)	H ₂ (sccm)	As. factor	Threshold	Smooth. factor	Iterations	Relative STD
200	0	0.001	0.04	7	400	14%
25	25	0.001	0.04	7	400	30%
25	0	0.001	0.02	7	400	19%
20	20	0.001	0.04	7	400	17%

5.4 Dual Furnace CVD

5.4.1 First Experimental Series

The optical microscope images of the samples are shown in Figures 5.4.2 and 5.4.1. The importance of the separate H_2 annealing step is clear from the etch marks in Figure 5.4.2d. Increasing the pressure to 150 Torr during the anneal also resulted in a smoother surface than at 100 Torr, as can be seen by comparing the sample in Figure 5.4.2e with the rest. Some particles seem to be sitting in the middle of the etch pits for this sample. However, the surface could also have been altered by the deposition step after annealing. The cleaning steps applied to these samples resulted in generally clean and homogeneous surfaces. Unfortunately, the spots on the microscope lens are clearly visible again.



(a) 10 sccm CH_4 and 10 sccm H_2 and 1 Torr.



(b) 10 sccm CH_4 and 10 sccm H_2 and 100 Torr.

Figure 5.4.1: Optical microscope images of graphene on Ge(110) samples grown by dual furnace CVD, 1st furnace temperature 1000 °C, 2nd furnace temperature 800 °C, 100x magnification and 4 μm scale bar.

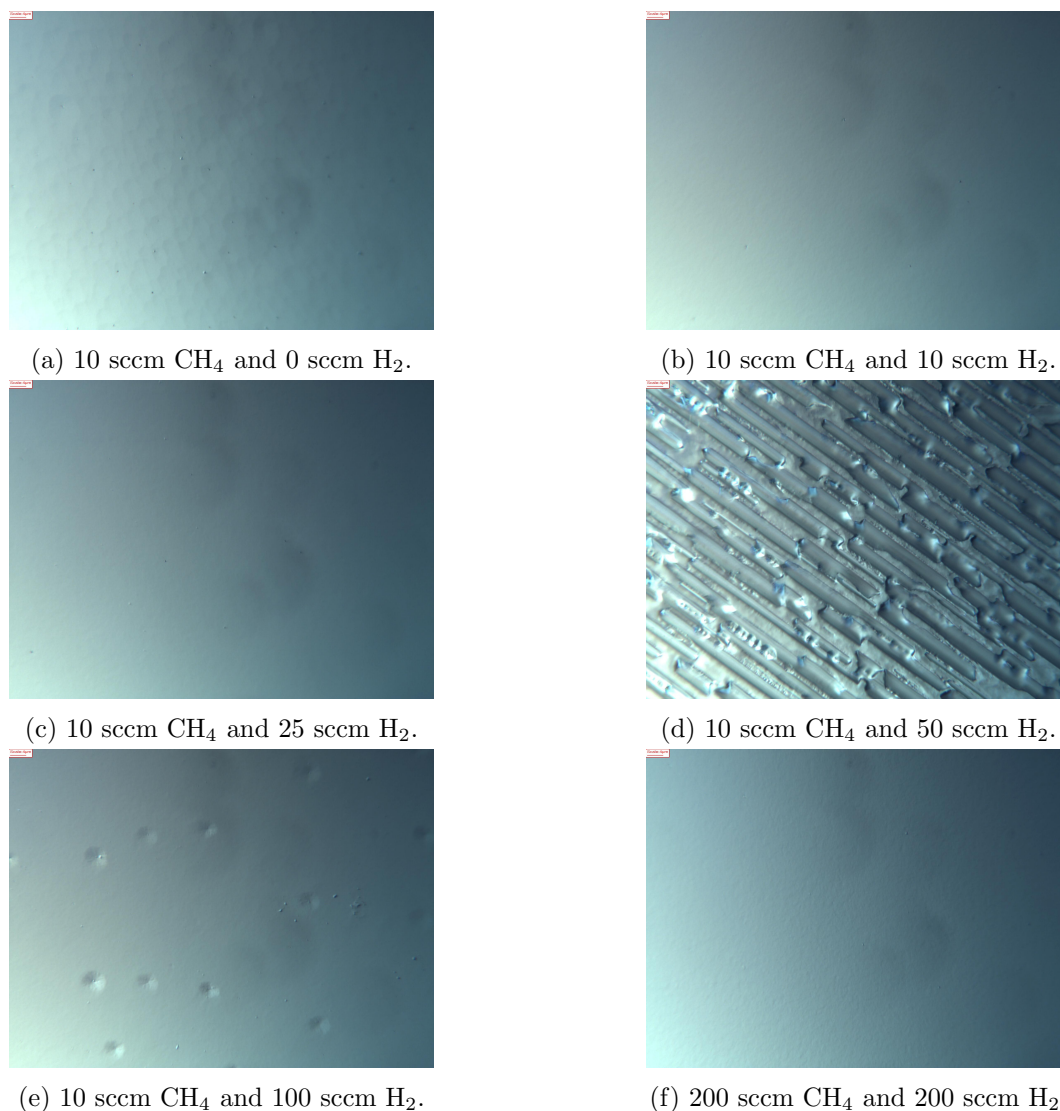


Figure 5.4.2: Optical microscope images of graphene on Ge(110) samples grown at 10 Torr pressure by dual furnace CVD, 1st furnace temperature 1000 °C, 2nd furnace temperature 800 °C, 100x magnification and 4 μm scale bar.

The averaged Raman spectra of the samples produced in the first series of dual furnace CVD experiments are shown in Figure 5.4.3. The measurement and analysis were performed in the same way as for the single furnace CVD series, see section 5.2. The relative standard deviation of the averaged spectra is given in Table 5.9. The background subtraction parameters were the same for all spectra, with an asymmetric factor of 0.001, a threshold of 0.03, a smoothing factor of 7, and a number of iterations of 400 for the asymmetric least square method. The D, G, O₂ and N₂ peaks are again visible in all samples and the D' is also clearly visible in many samples. On three samples

highly defective graphene may have been deposited due to the weak 2D peak for $\text{CH}_4:\text{H}_2 = 10:10$ sccm at 1 and 10 Torr and for $\text{CH}_4:\text{H}_2 = 10:25$ sccm at 10 Torr. Interestingly, a H_2/CH_4 ratio of 1 gives the best results at low pressures, which is not common in the literature and almost contradicts it. The weak 2D peak is not consistent with monolayer graphene, so it is likely that a thin layer of graphite was deposited. It could be that the high temperature of 1000 °C of the first furnace greatly increased the deposition rate, making the CH_4 decomposition more effective. On the other hand, a higher H_2 flow rate could help to decrease the deposition rate again and etch away parts, but these samples show no 2D peak at all. On the rest of the samples a mixture of amorphous carbon, graphite and highly defective graphene has probably been deposited again. The peaks in the spectrum of the samples showing a 2D peak were again fitted with a Lorentz function, the parameters and their standard errors are listed in Tables 5.10, 5.11 and 5.12. With the derived peak height parameters, the I_D/I_G ratios were calculated to be 2.5 ± 0.3 , 2.9 ± 0.3 and 2.7 ± 0.3 , and the I_{2D}/I_G ratio to be 0.37 ± 0.08 , 0.63 ± 0.08 and 0.61 ± 0.08 , for $\text{CH}_4:\text{H}_2 = 10:10$ sccm at 1 and 10 Torr and for $\text{CH}_4:\text{H}_2 = 10:25$ sccm at 10 Torr, respectively. Uncertainty estimates were calculated using the relative standard deviation of the averaged spectrum or the standard error of the parameters for the peaks, whichever is greater, and the propagation of uncorrelated uncertainty.

5 Results

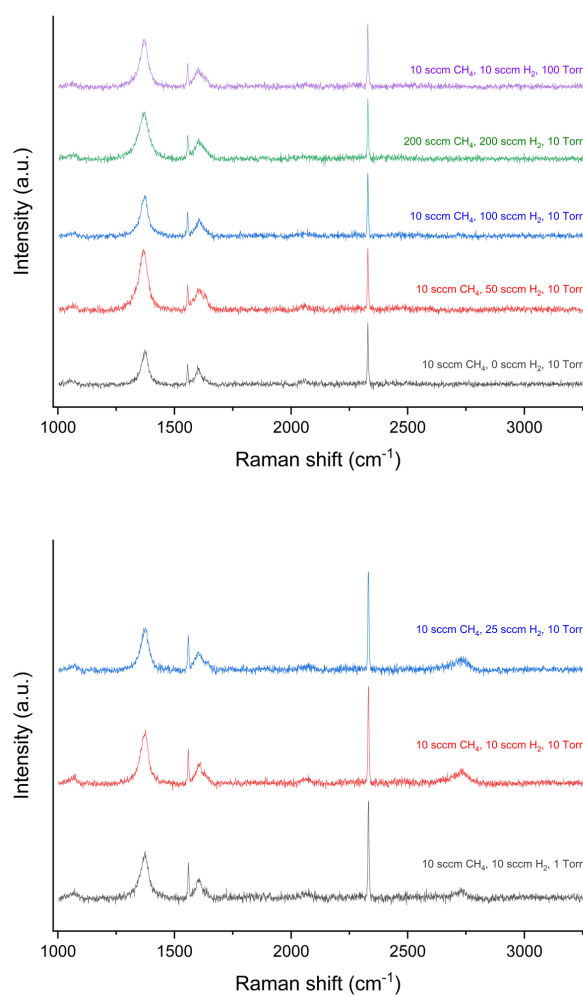


Figure 5.4.3: Averaged Raman spectra of graphene on Ge(110) samples grown by double furnace CVD, 1st furnace temperature 1000 °C, 2nd furnace temperature 800 °C.

Table 5.9: Relative standard deviation for the averaged Raman spectra of graphene on Ge(110) samples grown with dual furnace CVD, 1st furnace temperature 1000 °C, 2nd furnace temperature 800 °C.

Pressure (Torr)	H ₂ (sccm)	CH ₄ (sccm)	Relative STD
10	0	10	8%
10	10	10	6%
10	25	10	6%
10	50	10	30%
10	100	10	10%
10	200	200	9%
1	10	10	7%
100	10	10	7%

Table 5.10: Lorentz function fit parameters y-offset, peak center, area, FWHM and derived peak height and their standard errors for CH₄:H₂ = 10:10 sccm at 1 Torr grown by dual furnace CVD, 1st furnace temperature 1000 °C, 2nd furnace temperature 800 °C.

Peak	y_0	x_c	w	A	H
D	0.0748 ± 0.0011	1371.5 ± 0.6	37.8 ± 1.6	24.5 ± 0.8	0.413 ± 0.012
G	0.0748 ± 0.0011	1603.8 ± 1.2	31 ± 4	7.9 ± 0.7	0.164 ± 0.013
D'	0.0748 ± 0.0011	1639.3 ± 1.0	2 ± 3	0.15 ± 0.15	0.06 ± 0.05
2D	0.0748 ± 0.0011	2727 ± 4	36 ± 11	3.4 ± 0.7	0.060 ± 0.012

Table 5.11: Lorentz function fit parameters y-offset, peak center, area, FWHM and derived peak height and their standard errors for CH₄:H₂ = 10:10 sccm at 10 Torr grown by dual furnace CVD, 1st furnace temperature 1000 °C, 2nd furnace temperature 800 °C.

Peak	y_0	x_c	w	A	H
D	0.0738 ± 0.0011	1371.2 ± 0.5	35.9 ± 1.3	27.8 ± 0.7	0.493 ± 0.012
G	0.0738 ± 0.0011	1604.6 ± 1.6	32 ± 5	8.5 ± 1.1	0.168 ± 0.013
D'	0.0738 ± 0.0011	1631 ± 3	11 ± 11	0.7 ± 0.7	0.04 ± 0.03
2D	0.0738 ± 0.0011	2727 ± 3	62 ± 8	10.2 ± 1.0	0.105 ± 0.009

Table 5.12: Lorentz function fit parameters y-offset, peak center, area, FWHM and derived peak height and their standard errors for $\text{CH}_4:\text{H}_2 = 10:25$ sccm at 10 Torr grown dual furnace CVD, 1st furnace temperature 1000 °C, 2nd furnace temperature 800 °C

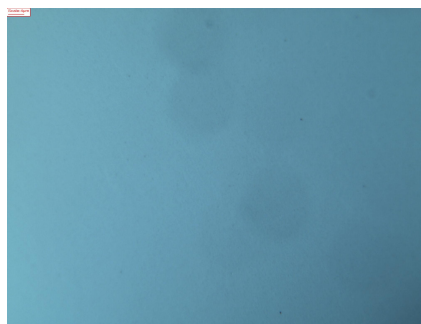
Peak	y_0	x_c	w	A	H
D	0.0625 ± 0.0012	1372.7 ± 0.6	35.3 ± 1.6	22.2 ± 0.7	0.400 ± 0.012
G	0.0625 ± 0.0012	1601.8 ± 1.8	45 ± 6	10.4 ± 1.0	0.148 ± 0.011
D'	0.0625 ± 0.0012	1644 ± 3	8 ± 9	0.4 ± 0.4	0.04 ± 0.03
2D	0.0625 ± 0.0012	2724 ± 3	63 ± 10	8.9 ± 1.0	0.090 ± 0.009

5.4.2 Second Experimental Series

The optical microscope images of the samples are shown in Figure 5.4.4. Except for the etch pits on the sample that was cleaned only with the standard degreasing method and not with the UV ozone cleaner and the additional H₂ annealing step, and the stains on the microscope lens, nothing is noticeable on the surface of the produced samples.



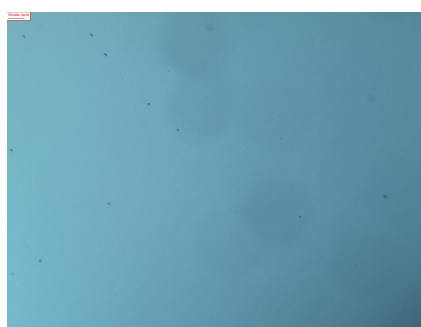
(a) Cleaned only with the standard degreasing method, 2nd furnace temperature 800 °C.



(b) 2nd furnace temperature 800 °C.



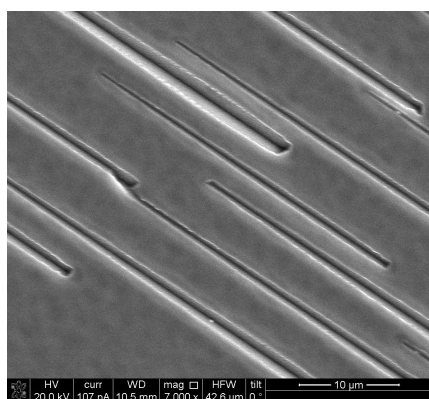
(c) 1st furnace temperature 800 °C, 2nd furnace temperature 800 °C.



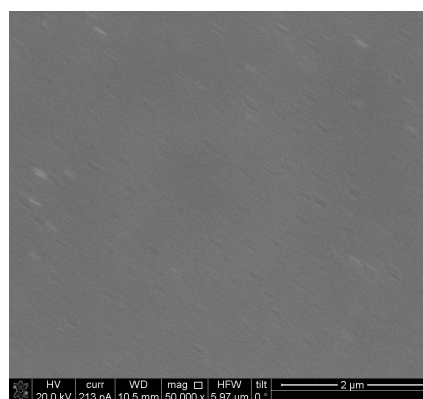
(d) 1st furnace temperature 1000 °C, 2nd furnace temperature 800 °C.

Figure 5.4.4: Optical microscope images of graphene on Ge(110) samples grown by dual furnace CVD, 100x magnification and 4 μm scale bar.

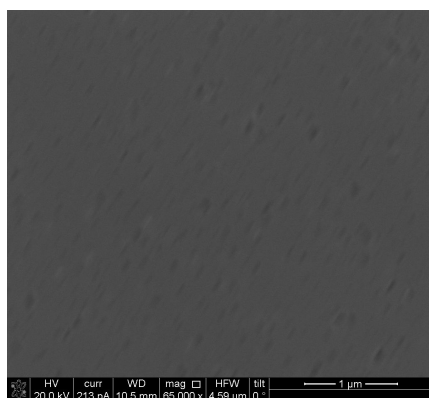
The SEM images of the samples are shown in Figure 5.4.5. No graphene flakes are clearly visible in the images. The etch pits are more clearly visible. Small holes are also visible on the other samples where the furnace temperatures did not exceed 800 °C. They could represent small etch pits, their shape does not really show any regularity and they do not seem to be deep. However, they also show a preferred orientation similar to the etch pits. An exact determination of their origin is not possible from the SEM images alone. On the sample where the first furnace was set at 1000 °C, a local deposition of some particles is visible.



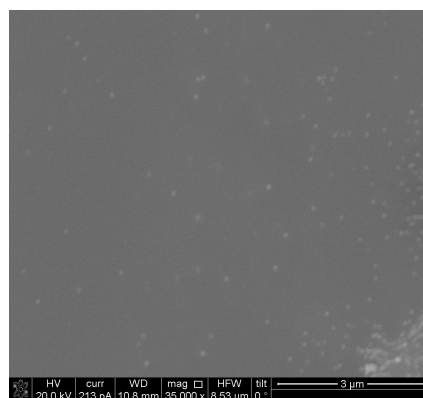
(a) Cleaned only with the standard degreasing method, 2nd furnace temperature 800 °C, 10 μm scale bar.



(b) 2nd furnace temperature 800 °C, 2 μm scale bar.



(c) 1st furnace temperature 800 °C, 2nd furnace temperature 800 °C, 1 μm scale bar.



(d) 1st furnace temperature 1000 °C, 2nd furnace temperature 800 °C, 3 μm scale bar.

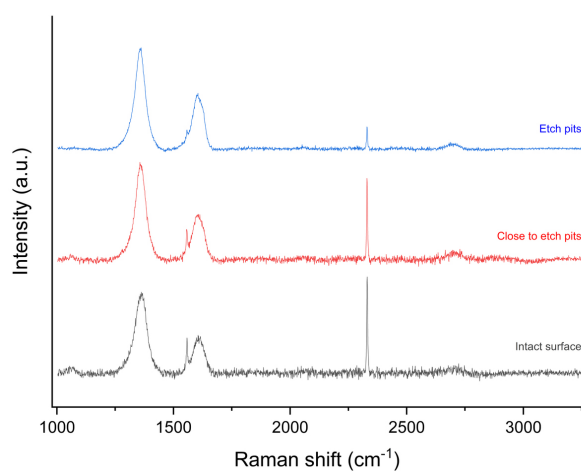
Figure 5.4.5: SEM images of graphene on Ge(110) samples grown by dual furnace CVD.

The averaged Raman spectra of the samples produced in the second series of experiments with dual furnace CVD are shown in Figure 5.4.6. The measurement and analysis were performed in the same way as for the CVD series, see section 5.2. The background subtraction parameters were the same for all spectra with an asymmetric factor of 0.001, a threshold of 0.04, a smoothing factor of 7, and a number of iterations of 400 for the asymmetric least square method. The D, G, O₂ and N₂ peaks are again visible in all samples. The sample reproduced from the previous single furnace CVD experiments was only cleaned with the standard degreasing method and therefore showed etch pits. The Raman spectra were again recorded with the laser focused on the intact surface and the etch pits, as well as in the vicinity of the etch pits. In the vicinity of the etch pits and in the etch pits, a 2D peak is again visible in the Raman spectra, and highly defective graphene has probably been deposited

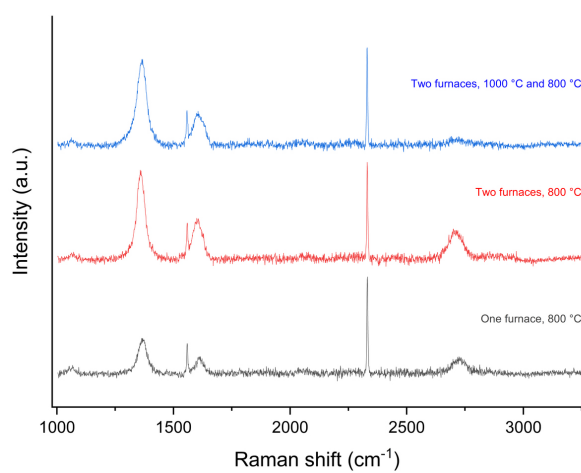
again. The peaks in both spectra were again fitted with a Lorentz function, the parameters for the fits and their standard errors are listed in Tables 5.13 and 5.14. The relative standard deviation for the averaged spectra is 8% for the intact surface, 10% near the etch pits, and 13% at the etch pits. Using the derived peak heights of the spectrum near the etch pits, the I_D/I_G ratio was calculated to be 2.2 ± 0.4 and the I_{2D}/I_G ratio was calculated to be 0.14 ± 0.03 . Using the derived peak heights of the spectrum at the etch pits, the I_D/I_G ratio was calculated to be 1.8 ± 0.4 and the I_{2D}/I_G ratio was calculated to be 0.093 ± 0.019 . The uncertainties were estimated using the relative standard deviation of the averaged spectra, since these values were larger than the standard errors of the derived parameters, and the propagation of uncorrelated uncertainty.

The samples that were also cleaned with the UV ozone cleaner and the additional H_2 annealing step, and had one or two furnaces set to 800 °C, show prominent 2D peaks. The peaks were also fitted with Lorentz functions, and the parameters for the fit and their standard errors are listed in Tables 5.15 and 5.16. Using the derived peak heights of the spectrum with one furnace at 800 °C, the I_D/I_G ratio was calculated to be 2.4 ± 0.4 and the I_{2D}/I_G ratio was calculated to be 0.95 ± 0.14 . Using the derived peak heights of the spectrum with both furnaces at 800 °C, the I_D/I_G ratio was calculated to be 2.2 ± 0.6 and the I_{2D}/I_G ratio was calculated to be 0.69 ± 0.18 . Uncertainties were estimated using the relative standard deviation of the averaged spectra, since these values were larger than the standard errors of the fitting parameters and the propagation of uncorrelated uncertainty. The additional cleaning steps not only result in a smoother surface, but also seem to be an important factor for graphene deposition. The relative standard deviation for the averaged Raman spectra is 10% and 17% for one 800 °C furnace and two 800 °C furnaces, respectively. The small nm-scale holes on the surface of the samples, visible on the SEM images in Figure 5.4.5, may be part of the reason for the prominent D peak in the Raman spectra. The I_{2D}/I_G ratios and the FWHM of the 2D peaks suggest that the obtained graphene film is thinner when only one furnace is used, at least when each other parameter is kept constant. However, the lower I_D/I_G ratio for the case of two furnaces suggests that fewer defects are introduced in the obtained film when both furnaces are used.

When the first furnace was set at 1000 °C, no clear 2D peak is visible. The relative standard deviation for the averaged spectra is 10%. The high temperatures of the first furnace seem to prevent graphene deposition, probably resulting in a mixture of amorphous carbon, graphite and highly defective graphene, similar to the intact surface of the first sample.



(a) Cleaned only by the standard degreasing method, 2nd furnace temperature 800 °C.



(b) Cleaned by the standard degreasing method, UV ozone cleaner and additional H₂ annealing step.

Figure 5.4.6: Averaged Raman spectra of graphene on Ge(110) samples grown by dual furnace CVD.

Table 5.13: Lorentz function fit parameters y-offset, peak center, area, FWHM, and derived peak height and their standard errors for the sample cleaned by the degreasing method only, grown by single furnace CVD at 800 °C, near the etch pits.

Peak	y_0	x_c	w	A	H
D	0.0611 ± 0.0011	1358.6 ± 0.3	46.5 ± 0.7	69.5 ± 0.8	0.951 ± 0.010
G	0.0611 ± 0.0011	1605.0 ± 0.5	48.3 ± 1.4	34.5 ± 0.8	0.455 ± 0.009
2D	0.0611 ± 0.0011	2707 ± 5	88 ± 14	8.9 ± 1.1	0.064 ± 0.007

Table 5.14: Lorentz function fit parameters y-offset, peak center, area, FWHM, and derived peak height and their standard errors for the sample cleaned by the degreasing method only, grown by single furnace CVD at 800 °C, etch pits.

Peak	y_0	x_c	w	A	H
D	0.0213 ± 0.0006	1356.35 ± 0.12	46.7 ± 0.4	72.9 ± 0.4	0.993 ± 0.005
G	0.0213 ± 0.0006	1605.1 ± 0.3	45.5 ± 0.7	39.4 ± 0.4	0.551 ± 0.005
2D	0.0213 ± 0.0006	2696 ± 3	71 ± 9	5.6 ± 0.6	0.051 ± 0.005

Table 5.15: Lorentz function fit parameters y-offset, peak center, area, FWHM, and derived peak height and their standard errors for the sample grown by single furnace CVD at 800 °C.

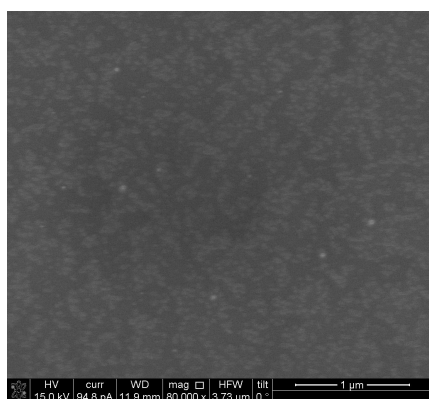
Peak	y_0	x_c	w	A	H
D	0.0776 ± 0.0011	1367.1 ± 0.7	37.5 ± 1.8	20.0 ± 0.7	0.338 ± 0.011
G	0.0776 ± 0.0011	1610.5 ± 1.5	35 ± 5	7.9 ± 0.7	0.140 ± 0.012
2D	0.0776 ± 0.0011	2725 ± 2	60 ± 6	12.5 ± 0.9	0.133 ± 0.009

Table 5.16: Lorentz function fit parameters y-offset, peak center, area, FWHM, and derived peak height and their standard errors for the sample grown by dual furnace CVD , 1st furnace temperature 800 °C, 2nd furnace temperature 800 °C.

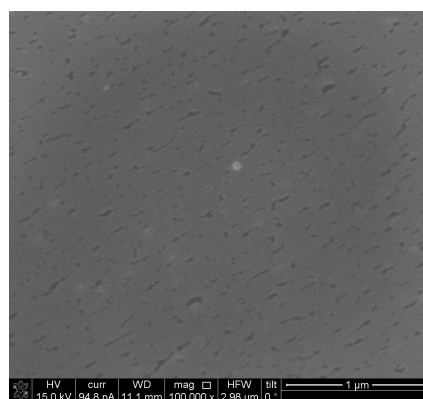
Peak	y_0	x_c	w	A	H
D	0.0715 ± 0.0012	1359.7 ± 0.3	37.0 ± 0.8	50.1 ± 0.8	0.862 ± 0.012
G	0.0715 ± 0.0012	1601.7 ± 0.6	43.9 ± 1.8	26.6 ± 0.8	0.386 ± 0.011
2D	0.0715 ± 0.0012	2710.1 ± 1.1	63 ± 4	27.0 ± 1.0	0.272 ± 0.009

5.4.3 Third Experimental Series

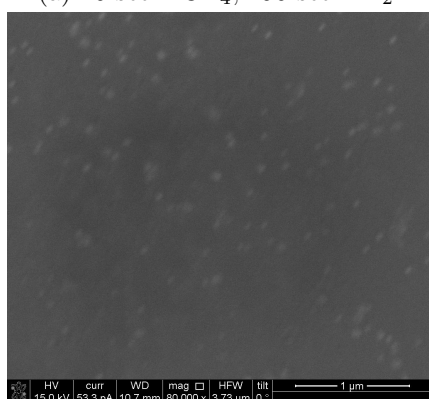
The obtained SEM images of the samples grown with different H_2/CH_4 ratios are shown in Figure 5.4.7, those with different deposition times in Figure 5.4.8, those at different pressures in Figure 5.4.9 and those at different deposition temperatures in Figure 5.4.10. The quality of the SEM images varies, the chosen acceleration voltage was either 10 or 15 kV. This voltage was too high and damaged the samples, voltages of 0.5 kV should be able to prevent this, but no good images could be obtained at this voltage. On many of the samples, the dark, small marks are noticeable again. These are probably etch pits, since they are also visible on samples where the Raman spectra suggest that no graphene has been obtained, and their density is lower where the Raman bands suggest a better quality of graphene. The surface of the sample grown at 10 sccm CH_4 and 190 sccm H_2 , shown in Figure 5.4.7a, looks like grain domains (lighter contrast) on a darker surface. However, graphene domains are usually darker than the Ge surface in SEM images, and the Raman spectra of this sample do not suggest that graphene was deposited on this sample. Another striking feature is the bright spot-like marks on many samples, which could be due to surface impurities. The 10 and 100 Torr experiments were performed twice, but the resulting Raman spectra did not change, and only one sample is shown. The experiment at 800 °C with 100 sccm CH_4 and 100 sccm H_2 at 0.8 Torr for 60 minutes was reproduced from the second series of experiments, but the resulting graphene quality was worse than before and the sample from the second series was used for the analysis. The data of this sample is used in the time series for 60 minutes and in the pressure series for 0.8 Torr. The data of the sample grown for 40 minutes at 800 °C with 100 sccm CH_4 and 100 sccm H_2 at 0.8 Torr is used in the time series for 40 minutes, in the H_2/CH_4 ratio series for a H_2/CH_4 ratio of 1 and in the temperature series for 800 °C.



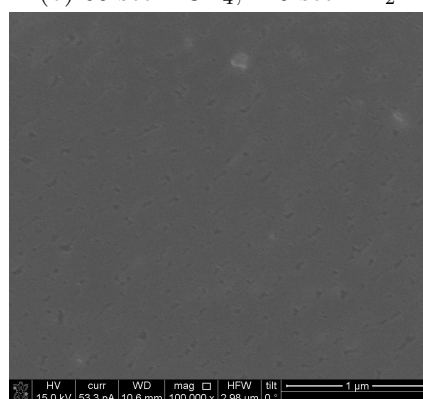
(a) 10 sccm CH₄, 190 sccm H₂.



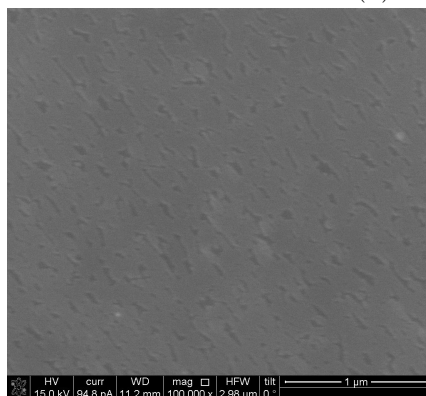
(b) 60 sccm CH₄, 140 sccm H₂.



(c) 140 sccm CH₄, 60 sccm H₂.

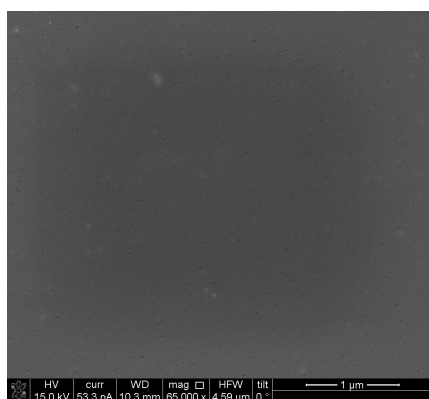


(d) 190 sccm CH₄, 10 sccm H₂.

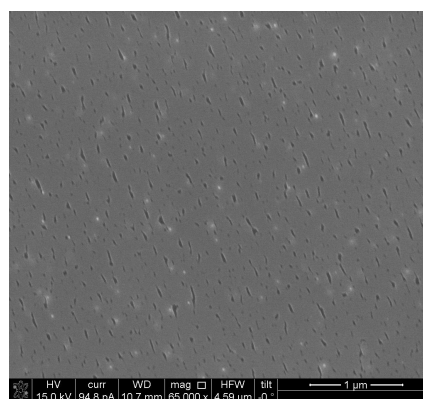


(e) 200 sccm CH₄, 0 sccm H₂.

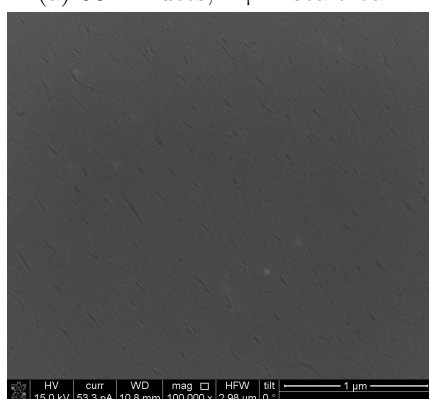
Figure 5.4.7: SEM images of graphene on Ge(110) samples grown by dual furnace CVD, H₂/CH₄ ratio series, 1 μm scale bar.



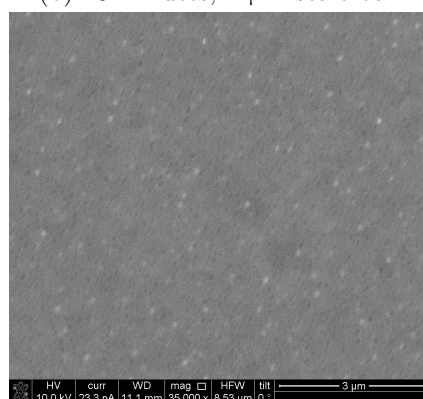
(a) 50 minutes, 1 μm scale bar.



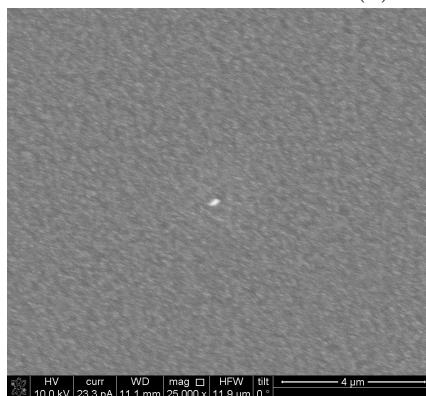
(b) 40 minutes, 1 μm scale bar.



(c) 30 minutes, 1 μm scale bar.

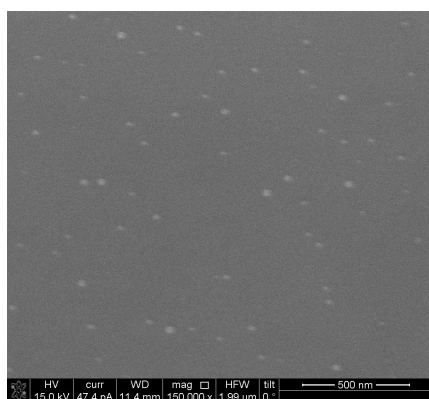


(d) 20 minutes, 3 μm scale bar.

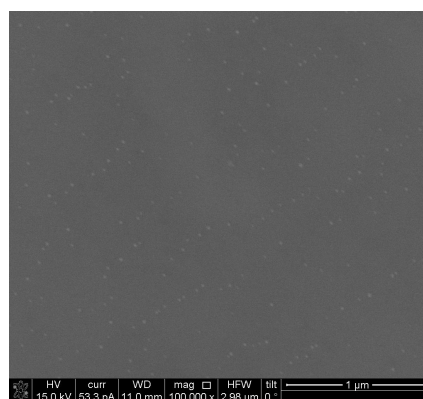


(e) 5 minutes, 4 μm scale bar.

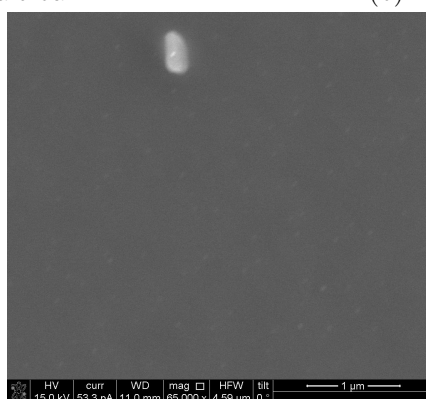
Figure 5.4.8: SEM images of graphene on Ge(110) samples grown by dual furnace CVD, time series.



(a) 760 Torr, 500 nm scale bar.



(b) 100 Torr, 1 μm scale bar.



(c) 10 Torr, 1 μm scale bar.

Figure 5.4.9: SEM images of graphene on Ge(110) samples grown by dual furnace CVD, pressure series.

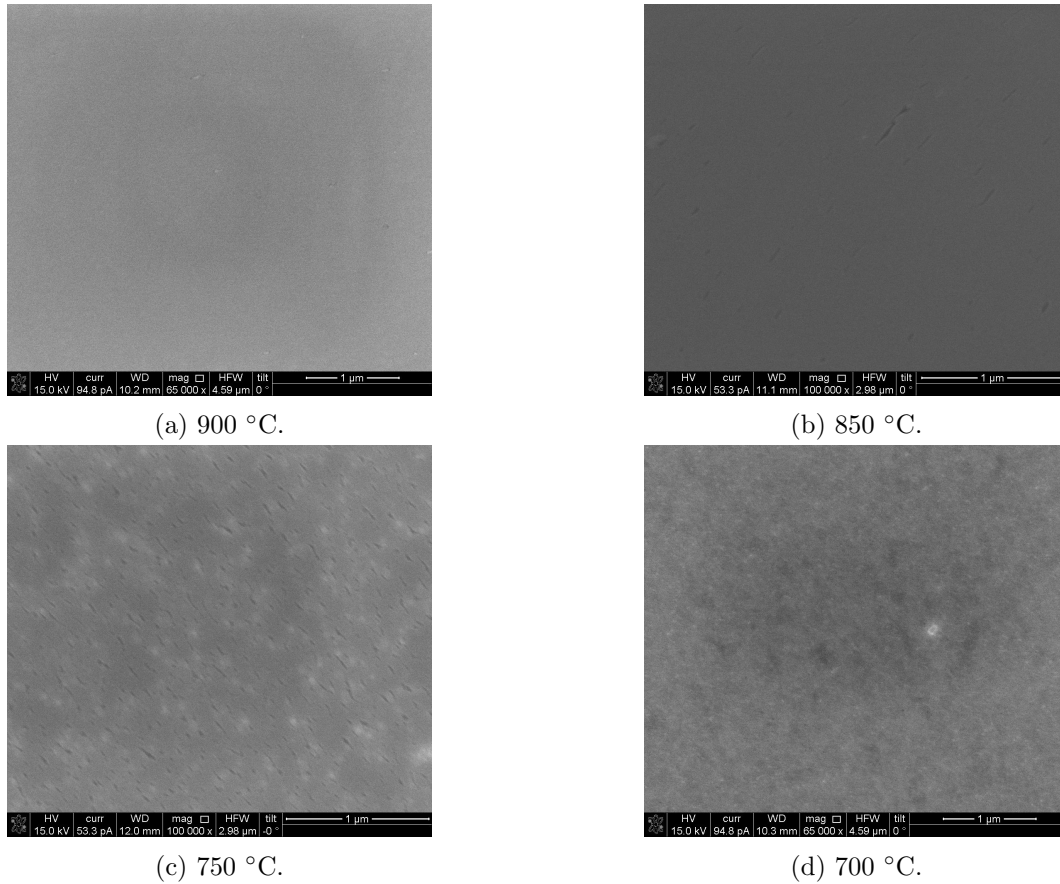


Figure 5.4.10: SEM images of graphene on Ge(110) samples grown by dual furnace CVD, temperature series, 1 μm scale bar.

The obtained averaged Raman spectra of the samples grown with different H_2/CH_4 ratios are shown in Figure 5.4.11, those with different deposition times in Figure 5.4.13, those at different pressures in Figure 5.4.15, and those at different deposition temperatures in Figure 5.4.16. The measurement and analysis were performed in the same way as for the single furnace CVD series, see section 5.2. The parameters for the correction of the germanium background with the asymmetric least square method are listed together with the relative standard deviation in Tables 5.18, 5.20, 5.21 and 5.23. The D peak, O_2 and N_2 peaks are again visible in all spectra. The G band is also visible in all spectra except for the sample from the H_2/CH_4 ratio series with 10 sccm CH_4 and 190 sccm H_2 . For many samples a 2D band was also obtained, these spectra were again fit with a Lorentz function, the parameters for the fits and their standard errors are listed in Tables 5.17, 5.19 and 5.22. The derived peak heights were used to calculate the I_D/I_G ratio and the I_{2D}/I_G ratio. Uncertainties were estimated using the relative standard deviation of the averaged spectrum or the standard error of the derived height for the peaks, whichever was greater, and the propagation of uncorrelated uncertainty. The values obtained are shown in Figures 5.4.12, 5.4.14 and 5.4.17. The results are ambiguous.

Usually a low I_D/I_G ratio corresponds to a high I_{2D}/I_G ratio and a low FWHM of the 2D band. However, this is not the case for the H_2/CH_4 ratio series and the time series.

For the H_2/CH_4 ratio series, the I_D/I_G ratios and the I_{2D}/I_G ratios suggest that the best graphene quality with fewer defects was achieved with 200 sccm CH_4 and 0 sccm H_2 . However, the FWHMs of the 2D bands are lowest for 140 sccm CH_4 and 60 sccm H_2 .

For the time series, the I_D/I_G ratio is lowest for the sample with a deposition time of 60 minutes, the I_{2D}/I_G ratio is highest for the sample with a deposition time of 40 minutes, and the FWHM of the 2D band is lowest for the sample with a deposition time of 30 minutes. Only in the temperature series the best result was clearly obtained at 900 °C. Also the pressure series has a winner, since only 0.8 Torr lead to the formation of graphene.

The reasons for the quality of these results are not only the few sample points, but also the low quality of the highly defective graphene films produced. In addition, focusing the laser on the samples to maximize the 2D band in the spectra often produced spectra that differed greatly from spectra with the laser focused on the surface and was a subjective process. Another factor was some misalignment in the Raman system, which resulted in low counts and low signal-to-noise ratio. To obtain good quality graphene, temperatures above 900 °C and low deposition rates due to a high H_2/CH_4 ratio with long deposition times are necessary, as also concluded in the literature and described in chapter 2.2.1. Furthermore, cooling with H_2 flow or annealing the samples after growth in different atmospheres could improve the results. Thus, the installation of a second furnace did not lead to the formation of high quality graphene at lower deposition temperatures, at least in the parameter range investigated.

Equations have been experimentally derived to estimate the average distance between structural defects with Raman spectra for the case of average distances greater than 10 nm and the case of average distances smaller than 3 nm, where the squared distance depends on the laser excitation energy in eV and the inverse or direct ratio of the peak intensity of the Raman D and G bands. The equations should be valid for a broad class of point defects that are Raman active, in the limit that only point defects contribute to the D band intensity. Alternatively, another empirical equation has been derived for only grain boundary defects contributing to the D band intensity, where the average size of crystalline grains can be estimated from the laser excitation energy in eV and the inverse ratio of the integrated intensity of the Raman D and G bands. Subsequently, the average density of point defects and graphene grains within the film can be estimated. (29) (38)

However, the quality of the produced graphene films and their Raman spectra is not good and probably point defects and grain boundaries contribute to the D band of the Raman spectra. The high I_D/I_G ratio suggests an average distance between structural defects smaller than 3 nm if only point defects would contribute to the D band intensity.

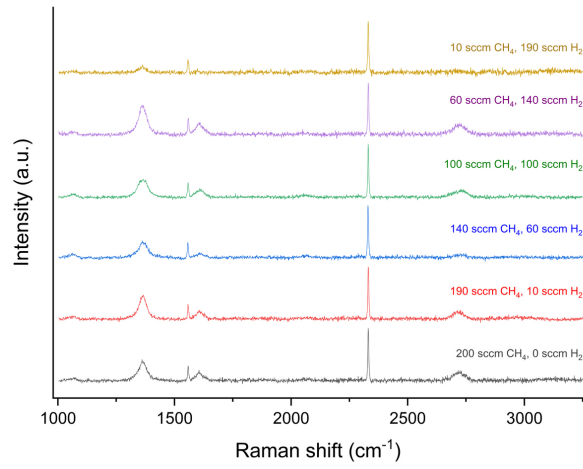


Figure 5.4.11: Averaged Raman spectra of graphene on Ge(110) samples grown by dual furnace CVD, H_2/CH_4 ratio series.

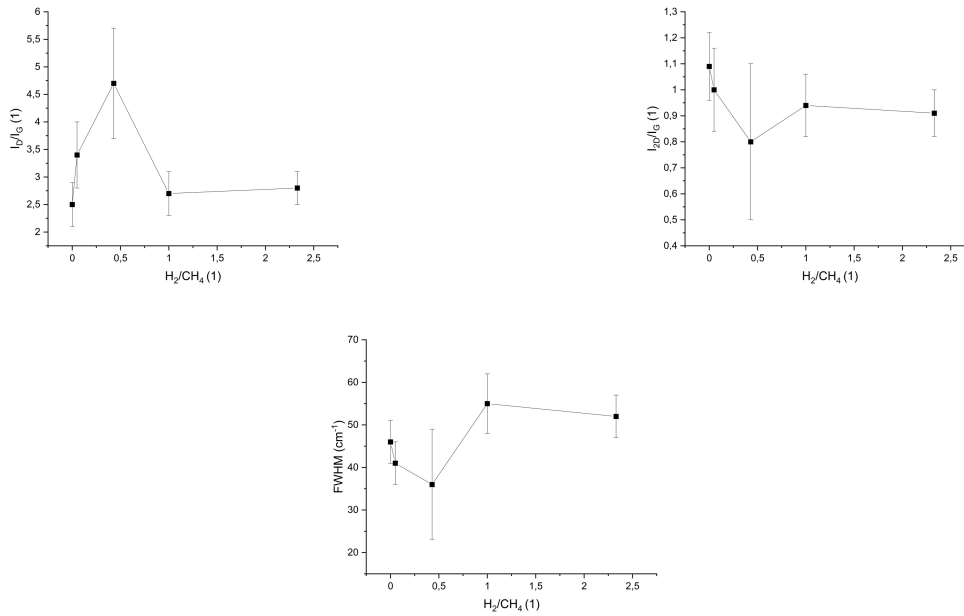


Figure 5.4.12: I_D/I_G ratios, I_{2D}/I_G ratios and FWHMs of the 2D peaks of the H_2/CH_4 ratio series. Error bars are σ .

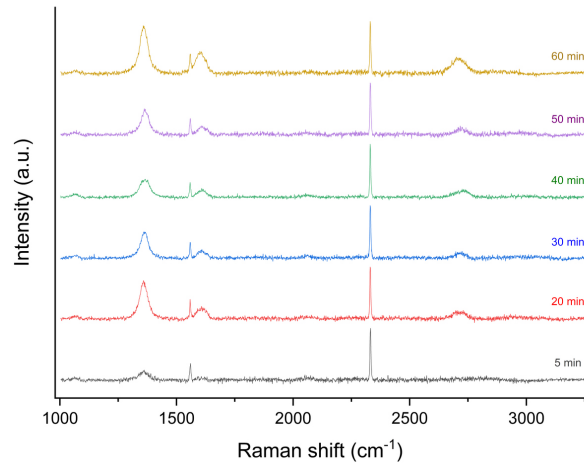


Figure 5.4.13: Averaged Raman spectra of graphene on Ge(110) samples grown by dual furnace CVD, time series.

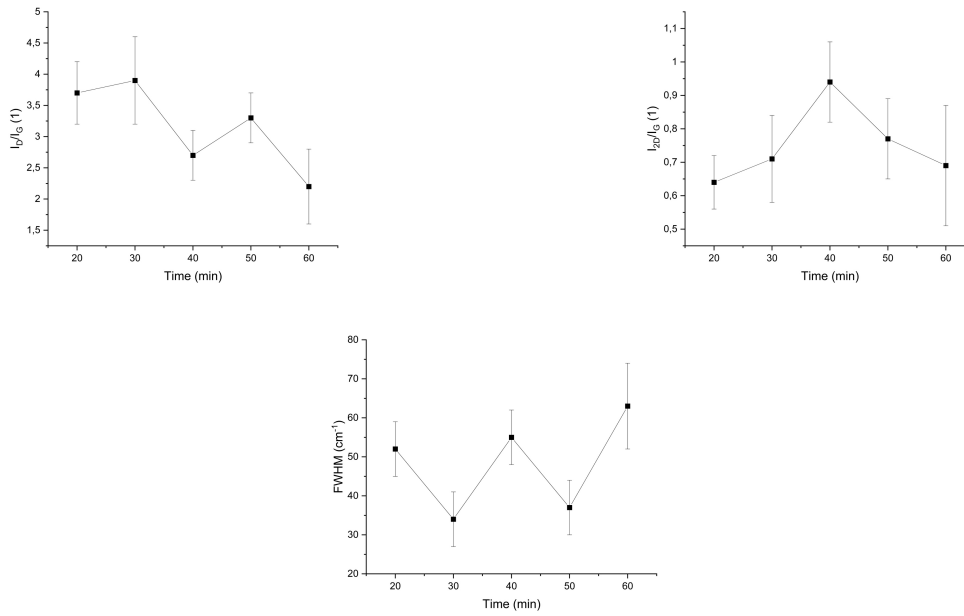


Figure 5.4.14: I_D/I_G ratios, I_{2D}/I_G ratios and FWHMs of the 2D peaks of the time series. Error bars are σ .

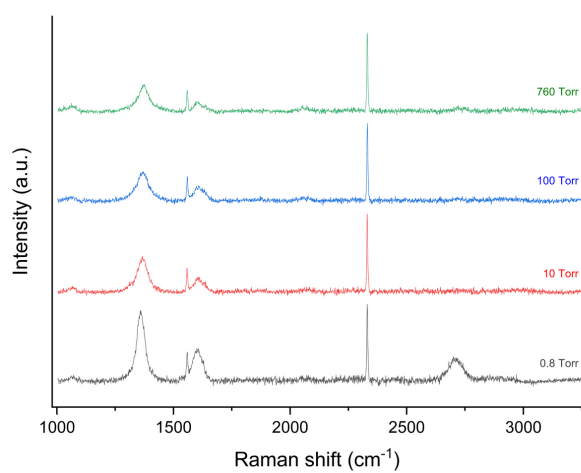


Figure 5.4.15: Averaged Raman spectra of graphene on Ge(110) samples grown by dual furnace CVD, pressure series.

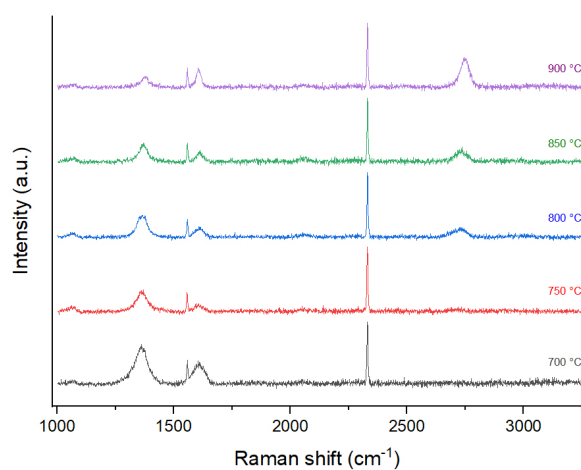


Figure 5.4.16: Averaged Raman spectra of graphene on Ge(110) samples grown by dual furnace CVD, temperature series.

5 Results

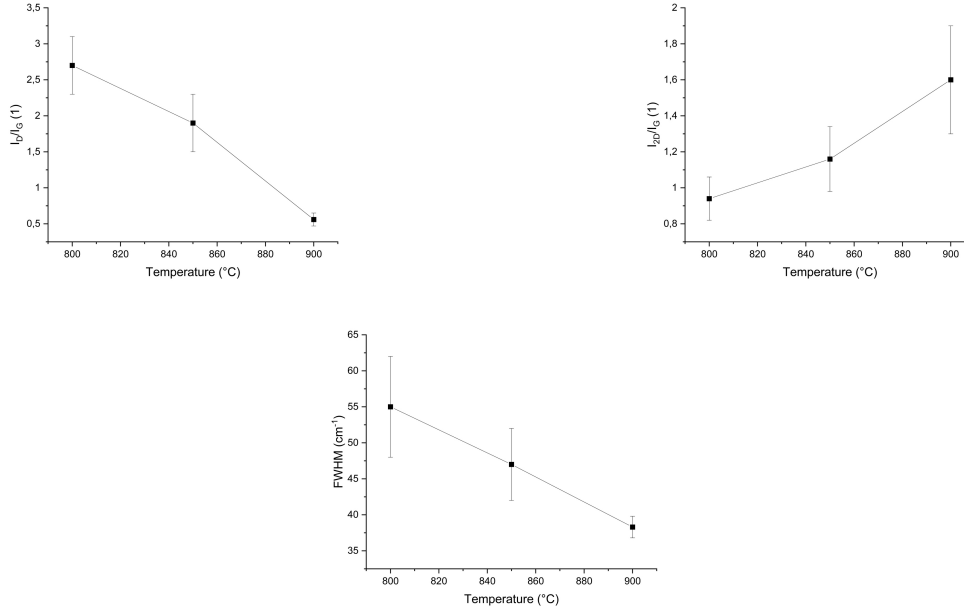


Figure 5.4.17: I_D/I_G ratios, I_{2D}/I_G ratios and FWHMs of the 2D peaks of the temperature series. Error bars are σ .

Table 5.17: Lorentz function fit parameters y-offset, peak center, area, FWHM, and derived peak height and their standard errors for the samples grown by dual furnace CVD, H_2/CH_4 ratio series.

H_2/CH_4 (1)	Peak	y_0	x_c	w	A	H
0	D	0.0694 ± 0.0011	1363.7 ± 0.6	36.0 ± 1.7	19.3 ± 0.7	0.342 ± 0.011
0	G	0.0694 ± 0.0011	1605.6 ± 1.4	32 ± 4	6.7 ± 0.7	0.135 ± 0.012
0	2D	0.0694 ± 0.0011	2719.7 ± 1.6	46 ± 5	10.6 ± 0.8	0.147 ± 0.010
0.05	D	0.0741 ± 0.0010	1363.9 ± 0.5	32.7 ± 1.3	21.8 ± 0.7	0.425 ± 0.012
0.05	G	0.0741 ± 0.0010	1606.8 ± 1.5	33 ± 5	6.4 ± 0.7	0.126 ± 0.012
0.05	2D	0.0741 ± 0.0010	2716.0 ± 1.7	41 ± 5	8.2 ± 0.8	0.126 ± 0.011
0.43	D	0.0739 ± 0.0011	1365.5 ± 0.8	40 ± 3	17.3 ± 0.7	0.276 ± 0.011
0.43	G	0.0739 ± 0.0011	1608 ± 4	35 ± 10	3.2 ± 0.7	0.059 ± 0.012
0.43	2D	0.0739 ± 0.0011	2727 ± 5	36 ± 13	2.5 ± 0.7	0.045 ± 0.012
2.33	D	0.0790 ± 0.0011	1363.3 ± 0.4	36.0 ± 1.2	30.0 ± 0.7	0.530 ± 0.012
2.33	G	0.0790 ± 0.0011	1606.1 ± 1.2	36 ± 4	10.7 ± 0.7	0.187 ± 0.012
2.33	2D	0.0790 ± 0.0011	2720.8 ± 1.5	52 ± 5	14.0 ± 0.9	0.171 ± 0.010

Table 5.18: Background subtraction parameters asymmetric factor, threshold, smoothing factor and number of iterations for asymmetric least square method and relative standard deviation for the averaged Raman spectra of graphene on Ge(110) samples grown by dual furnace CVD, H₂/CH₄ ratio series.

H ₂ /CH ₄ (1)	As. factor	Threshold	Smooth. factor	Iterations	Relative STD
0	0.001	0.03	7	400	6%
0.05	0.001	0.04	7	400	11%
0.43	0.001	0.03	7	400	6%
2.33	0.001	0.03	7	400	6%
19	0.001	0.04	7	400	6%

Table 5.19: Lorentz function fit parameters y-offset, peak center, area, FWHM, and derived peak height and their standard errors for the samples grown by dual furnace CVD, time series.

Time (min)	Peak	y_0	x_c	w	A	H
20	D	0.0774 ± 0.0012	1359.3 ± 0.45	35.5 ± 0.9	37.7 ± 0.7	0.677 ± 0.012
20	G	0.0774 ± 0.0012	1606.0 ± 1.3	42 ± 4	12.1 ± 0.8	0.183 ± 0.011
20	2D	0.0774 ± 0.0012	2712 ± 3	52 ± 7	9.7 ± 0.9	0.117 ± 0.010
30	D	0.0666 ± 0.0011	1362.8 ± 0.5	33.7 ± 1.3	25.4 ± 0.7	0.479 ± 0.012
30	G	0.0666 ± 0.0011	1607.1 ± 1.7	35 ± 5	6.8 ± 0.7	0.122 ± 0.012
30	2D	0.0666 ± 0.0011	2716 ± 3	34 ± 7	4.7 ± 0.7	0.087 ± 0.012
40	D	0.0552 ± 0.0011	1364.1 ± 0.7	42.3 ± 1.9	22.0 ± 0.8	0.330 ± 0.010
40	G	0.0552 ± 0.0011	1607.6 ± 1.7	40 ± 5	7.6 ± 0.7	0.122 ± 0.011
40	2D	0.0552 ± 0.0011	2727 ± 3	55 ± 7	10.0 ± 0.9	0.115 ± 0.009
50	D	0.0790 ± 0.0011	1365.0 ± 0.5	35.0 ± 1.4	24.3 ± 0.7	0.443 ± 0.012
50	G	0.0790 ± 0.0011	1608.5 ± 1.7	38 ± 5	7.9 ± 0.8	0.133 ± 0.012
50	2D	0.0790 ± 0.0011	2719 ± 3	37 ± 7	6.1 ± 0.8	0.103 ± 0.012

Table 5.20: Background subtraction parameters asymmetric factor, threshold, smoothing factor and number of iterations for asymmetric least square method and relative standard deviation for the averaged Raman spectra of graphene on Ge(110) samples grown by dual furnace CVD, time series.

Time (min)	As. factor	Threshold	Smooth. factor	Iterations	Relative STD
5	0.001	0.04	7	400	6%
20	0.001	0.05	7	400	8%
30	0.001	0.05	7	400	11%
40	0.001	0.04	7	400	7%
50	0.001	0.05	7	400	6%

Table 5.21: Background subtraction parameters asymmetric factor, threshold, smoothing factor and number of iterations for asymmetric least square method and relative standard deviation for the averaged Raman spectra of graphene on Ge(110) samples grown by dual furnace CVD, pressure series.

Pressure (Torr)	As. factor	Threshold	Smooth. factor	Iterations	Relative STD
10	0.001	0.04	7	400	12%
100	0.001	0.04	7	400	6%
760	0.001	0.02	7	400	7%

Table 5.22: Lorentz function fit parameters y-offset, peak center, area, FWHM, and derived peak height and their standard errors for the samples grown by dual furnace CVD, temperature series.

Temperature ($^{\circ}$ C)	Peak	y_0	x_c	w	A	H
850	D	0.0687 ± 0.0011	1369.2 ± 0.9	37 ± 3	14.3 ± 0.7	0.248 ± 0.011
850	G	0.0687 ± 0.0011	1610.5 ± 1.3	26 ± 4	5.3 ± 0.6	0.131 ± 0.014
850	2D	0.0687 ± 0.0011	2730.6 ± 1.5	47 ± 5	11.2 ± 0.8	0.152 ± 0.010
900	D	0.0656 ± 0.0010	1376.6 ± 1.3	33 ± 4	7.7 ± 0.7	0.152 ± 0.012
900	G	0.0656 ± 0.0010	1606.5 ± 0.6	20.8 ± 1.7	8.7 ± 0.5	0.265 ± 0.015
900	2D	0.0656 ± 0.0010	2748.0 ± 0.5	38.3 ± 1.5	26.0 ± 0.7	0.433 ± 0.011

Table 5.23: Background subtraction parameters asymmetric factor, threshold, smoothing factor and number of iterations for asymmetric least square method and relative standard deviation for the averaged Raman spectra of graphene on Ge(110) samples grown by dual furnace CVD, temperature series.

Temperature ($^{\circ}$ C)	As. factor	Threshold	Smooth. factor	Iterations	Relative STD
700	0.001	0.04	7	400	7%
750	0.001	0.03	7	400	7%
850	0.001	0.03	7	400	10%
900	0.001	0.03	7	400	10%

6 Conclusions and Outlook

The cleaning process of the Ge(110) samples was not constant during the experiments due to the simultaneous development. The best results were obtained with *ex-situ* cleaning steps consisting of ultrasonication in acetone for five minutes, ultrasonication in isopropanol for five minutes, six rinses with deionized water, and then gentle scraping of the germanium surface with a micro cleanroom swab in acetone, followed by ultrasonication in acetone for 15 minutes at 35 °C, ultrasonication in isopropanol for 15 minutes at 35 °C, six rinses with deionized water, and blow drying with N₂ followed by ten minutes in a UV ozone cleaner. The *in-situ* cleaning step consisted of a H₂ anneal for 30 minutes at 800 °C and 150 Torr with 200 sccm of H₂ flowing.

Graphene was successfully deposited on Ge(110) samples in preliminary chemical vapor deposition experiments at 800 °C, 100 sccm H₂ and 100 sccm CH₄ with a deposition time of 60 minutes at a pressure of 800 mTorr.

Deposition of graphene by plasma-enhanced chemical vapor deposition was not successful, probably because the base pressure was too high to achieve a stable plasma.

Chemical vapor deposition was performed with two furnaces to investigate the possibility of a lower graphene deposition temperature. Several series of experiments with parameter studies were performed. In preliminary experiments, low pressures in the range of 1 Torr to 10 Torr and H₂/CH₄ ratios close to 1 resulted in graphene deposition at 800 °C. A more extensive parameter study showed that H₂/CH₄ ratios below 2.4 resulted in graphene deposition, and using only CH₄ as precursor gave the best results in the parameter ranges investigated. The ideal deposition time could not be fully determined, but was in the range of 40 to 60 minutes in the experiments conducted. Graphene deposition could not be achieved at pressures higher than 800 mTorr. Deposition temperatures of 900 °C gave the best results, and no graphene could be deposited below 800 °C. The use of two furnaces in the CVD process did not demonstrate a clear improvement in graphene deposition and did not allow lower deposition temperatures in the context of this thesis.

Raman spectroscopy showed that the deposited graphene is highly defective and probably not monolayer graphene, so no ideal recipe was determined. Optical microscopy showed clean and smooth surfaces, but electron microscopy

revealed etch pits in the nm range.

The next step would be to further optimize the cleaning process to achieve clean and smooth surfaces without etch pits. In addition, different parameter ranges and post-deposition cooling processes should be investigated with reference to the literature to achieve high quality and monolayer graphene. This could be achieved by modifying the experimental setup.

Bibliography

1. M. Ohring, in (Elsevier Inc., Second Edition, 2002), chap. 4, 6, 8, pp. 145–201, 277–353, 427–492, ISBN: 978-0-12-524975-1.
2. M. Saeed, Y. Alshammari, S. A. Majeed, E. Al-Nasrallah, *Molecules* **25**, 3856 (Aug. 2020).
3. C. Kittel, in (John Wiley & Sons, Inc., Eighth, 2005), chap. 1, p. 17.
4. W. Demtröder, in (Springer-Verlag, five, 2016), chap. 11, p. 379, ISBN: 978-3-662-49093-8.
5. C. Mullet, S. Chiang, *Surface science* **621**, 184–190 (Mar. 2014).
6. R. C. Frank, J. Thomas Jr, *Journal of physics and chemistry of solids* **16**, 144–151 (1960).
7. Y. Dedkov, E. Voloshina, *Nanoscale* **12**, 11416–11426 (May 2020).
8. A. Becker, C. Wenger, J. Dabrowski, *Journal of Applied Physics* **126**, 085306 (Aug. 2019).
9. P. Ponath, A. B. Posadas, A. A. Demkov, *Applied Physics Reviews* **4**, 021308 (June 2017).
10. X.-J. Zhang *et al.*, *Journal of Vacuum Science & Technology A: Vacuum, Surfaces, and Films* **11**, 2553–2561 (Sept. 1993).
11. J. S. Hovis, R. J. Hamers, C. M. Greenlief, *Surface science* **440**, L815–L819 (Oct. 1999).
12. S. Gan *et al.*, *Surface science* **395**, 69–74 (Jan. 1998).
13. L. Chan, E. Altman, Y. Liang, *Journal of Vacuum Science & Technology A: Vacuum, Surfaces, and Films* **19**, 976–981 (May 2001).
14. P. Ponath, A. B. Posadas, R. C. Hatch, A. A. Demkov, *Journal of Vacuum Science & Technology B, Nanotechnology and Microelectronics: Materials, Processing, Measurement, and Phenomena* **31**, 031201 (Apr. 2013).
15. M. Walker, M. Tedder, J. Palmer, J. Mudd, C. McConville, *Applied Surface Science* **379**, 1–7 (Aug. 2016).
16. J. Cho, R. Nemanich, *Physical Review B* **46**, 12421 (Nov. 1992).
17. V. Loup *et al.*, presented at the Ultra Clean Processing of Semiconductor Surfaces VIII, vol. 134, pp. 37–40.
18. K. Choi, J. M. Buriak, *Langmuir* **16**, 7737–7741 (Aug. 2000).
19. J. Y. Kim, J. McVittie, K. Saraswat, Y. Nishi, presented at the Solid State Phenomena, vol. 134, pp. 33–36.

20. S. Rivillon, Y. J. Chabal, F. Amy, A. Kahn, *Applied Physics Letters* **87**, 253101 (Dec. 2005).
21. S. Sun *et al.*, *Applied Physics Letters* **88**, 021903 (Jan. 2006).
22. G. Anderson, M. Hanf, P. Norton, Z. Lu, M. Graham, *Applied physics letters* **66**, 1123–1125 (Feb. 1995).
23. H. Okumura, T. Akane, S. Matsumoto, *Applied surface science* **125**, 125–128 (Jan. 1998).
24. T. Akane, J. Tanaka, H. Okumura, S. Matsumoto, *Applied surface science* **108**, 303–305 (Feb. 1997).
25. H. Seo, K. Chung, J. Long, G. Lucovsky, *Journal of The Electrochemical Society* **156**, H813 (Sept. 2009).
26. J. Dai *et al.*, *Nano Letters* **16**, 3160–3165 (Apr. 2016).
27. M. Losurdo, M. M. Giangregorio, P. Capezzuto, G. Bruno, *Physical Chemistry Chemical Physics* **13**, 20836–20843 (Oct. 2011).
28. B. Kiraly *et al.*, *Nano letters* **15**, 7414–7420 (Oct. 2015).
29. R. M. Jacobberger *et al.*, *ACS Applied Nano Materials* **2**, 4313–4322 (June 2019).
30. R. M. Jacobberger *et al.*, *Chemistry of Materials* **34**, 6769–6778 (July 2022).
31. L. Persichetti *et al.*, *Applied Surface Science* **499** (Jan. 2020).
32. J.-H. Lee *et al.*, *Science* **344**, 286–289 (Apr. 2014).
33. B. Bekdüz, U. Kaya, M. Langer, W. Mertin, G. Bacher, *Scientific Reports* **10**, 12938 (July 2020).
34. A. Al-Hagri *et al.*, *Carbon* **155**, 320–325 (Dec. 2019).
35. X. Song *et al.*, *Materials Letters* **137**, 25–28 (Dec. 2014).
36. A. Malesevic *et al.*, *Nanotechnology* **19**, 305604 (June 2008).
37. J.-Y. Hwang, C.-C. Kuo, L.-C. Chen, K.-H. Chen, *Nanotechnology* **21**, 465705 (Oct. 2010).
38. A. C. Ferrari, D. M. Basko, *Nature nanotechnology* **8**, 235–246 (Apr. 2013).
39. P. H. Eilers, H. F. Boelens, *Leiden University Medical Centre Report* **1**, 5 (Oct. 2005).
40. S. He *et al.*, *Analytical Methods* **6**, 4402–4407 (Mar. 2014).
41. F. Qian *et al.*, *ACS Applied Materials & Interfaces* **14**, 53174–53182 (2022).